A NOVEL ROLE FOR THE RGS PROTEIN SST2 IN YEAST SIGNALING REVEALED BY MATHEMATICAL MODELING AND LIVE CELL IMAGING

Sai Phanindra Venkatapurapu

A dissertation submitted to the faculty of the University of North Carolina at Chapel Hill in partial fulfillment of the requirements for the degree of Doctor of Philosophy in the Curriculum in Bioinformatics and Computational Biology.

Chapel Hill
2014

Approved by:

Timothy C. Elston

Henrik G. Dohlman

Beverly Errede

Shawn M. Gomez

Patrick J. Brennwald

ABSTRACT

Sai Phanindra Venkatapurapu: A novel role for the RGS protein Sst2 in yeast signaling revealed by mathematical modeling and live cell imaging.
(Under the direction of Timothy C. Elston.)

G-protein coupled receptor (GPCR) signaling is fundamental to various cellular processes such as cardiac contractility, immune response and gradient sensing. Budding yeast, *Saccharomyces cerevisiae*, detect gradients of mating pheromone as shallow as 1-5% across their diameter and generate appropriate morphological response. Receptor polarization has been implicated in pheromone gradient sensing and recent work has suggested that endocytosis is important in establishing polarity of membrane proteins. However, the precise mechanisms that regulate the endocytosis of the receptor Ste2 to establish a polarized receptor distribution have not been fully characterized. The Regulator of G-protein Signaling (RGS) protein, Sst2, negatively regulates G-protein activity and facilitates mating pathway desensitization in yeast. It has been previously suggested that Sst2 interacts with the receptor Ste2 through its DEP domains. In the chapters that follow, we use an integrated approach that combines computational and experimental methods to demonstrate that following pheromone stimulation, Sst2 inhibits Ste2 endocytosis and stabilizes it at the plasma membrane. We also show that disrupting the binding interaction between Sst2 and Ste2 by a point mutation Q304N in Sst2 leads to loss of Ste2 polarization. Our mathematical model predicts pheromone-induced synthesis of Sst2 as a key factor in establishing Ste2 polarization. We verify this prediction by replacing the endogenous promoter of SST2 with a promoter that is not responsive to pheromone. Thus, in this work, we show that by inhibiting Ste2 endocytosis, Sst2 plays a positive role in the yeast pheromone response. By discovering a novel positive role for a negative regulator, this work has provided an improved understanding of how RGS proteins and GPCRs interact in yeast. GPCR signaling is a highly conserved pathway and RGS proteins bind GPCRs even

in mammalian systems. Therefore, the inhibition of GPCR internalization by RGS proteins could be of a general occurrence. Since RGS proteins are potential drug targets, in addition to GPCRs, an improved understanding of RGS-GPCR interaction, as provided in this work, will greatly benefit drug discovery.

Dedicated to my Mom, Dad and Sister for their love and tremendous support

and

Manjiri for taking good care of me during the crucial thesis writing-defense phase!

ACKNOWLEDGMENTS

This work would not have been possible with out the support of my advisors, Timothy Elston, Henrik Dohlman and Beverly Errede. I am grateful to the guidance they have provided over the past six years. Tim has been a really great mentor and I have learned a great deal about mathematical modeling and quantitative analysis from him. Henrik and Beverly have supported me in my experimental work by providing feedback, troubleshooting and suggesting experiments. Gauri Dixit and Matthew Pena have provided me the yeast strains used in the study. Gauri was also extremely helpful during my stints at the lab bench. I would like to thank Josh Kelley for his support throughout the project. Brainstorming with Josh and Gauri was extremely motivational and I will miss working with them. Josh has been instrumental in setting up the microscope facility for our lab use and he used to provide constructive feedback to make my talks and posters better. I would also like to thank all the members of the Elston lab, the Dohlman lab and the Errede lab for their support. Special thanks to Vinal Lakhani for bringing me home-made Indian food whenever he visited his folks. I would also like to thank the rest of my thesis committee - Patrick Brennwald and Shawn Gomez for giving me useful feedback and constructive criticism of my work during committee meetings. I learnt a lot on biological networks through the courses taught by Shawn Gomez. Working with Shawn was a great experience. I would like thank my friends and fellow students in the BCB curriculum for their support.

I am greatly indebted to my family for all love and support they have given me and the sacrifices they made to help me reach where I am now. Thank you Mom, Dad and Sis for everything you have given me. I will strive hard to make you feel proud!

TABLE OF CONTENTS

LIST OF FIGURES

LIST OF TABLES

LIST OF ABBREVIATIONS

G-protein	Guanosine nucleotide-binding protein
GDP	Guanosine diphosphate
GTP	Guanosine triphosphate
GPCR	G-protein couple receptor
RGS	Regulator of G-protein signaling
GEF	Guanine nucleotide exchange factor
GAP	GTPase activating protein
ODE	Ordinary Differential Equation
PI	Polarization Index

CHAPTER 1

INTRODUCTION

G-protein coupled receptors (GPCRs) comprise a large family of transmembrane proteins involved in many eukaryotic signaling processes including proper cardiac function, cell growth regulation and immune response [1, 2]. Dysfunction of GPCRs results in pathophysiology. GPCRs are the most common drug-targets in the pharmaceutical industry [3]. Recently, there has been a substantial focus on the Regulators of G-protein Signaling (RGS) proteins [4] as potential drug targets. RGS proteins are the main negative regulators of GPCR signaling. Besides serving as GTPase activating proteins (GAPs), RGS proteins bind to effectors, scaffold proteins and are also involved in effector regulation. Due to the roles they play in the pathogenesis of cardiac hypertrophy and hypertension, RGS proteins are potential therapeutic targets in cardiovascular diseases [5, 6, 7]. Recently RGS2 was identified as the negative regulator of β(2)AR-G(i) signaling, thus providing a potential target for the treatment of chronic heart failure [8, 9, 10]. Thus a detailed understanding of the roles of RGS proteins in GPCR signaling can result in the discovery of new pharmacological targets. Sst2, the founding member of the RGS family of proteins, is a negative regulator in the pheromone response pathway [11]. Here we identify a novel positive role for Sst2 in the pheromone pathway, which could be relevant to G-protein signaling pathways in other organisms.

1.1 Pheromone response pathway in yeast

Budding yeast, Saccharomyces cerevisiae exists stably as both haploids and diploids. Haploid yeast has two mating types - a and α [12]. a-cell secretes mating pheromone a-factor which is detected by α-cell and α-cell secretes α-factor detected by a-cell [13]. Depending on the concentration of pheromone, yeast either elongate in the direction of the mating partner or form a mating projection (shmoo) [14]. The mating projections, thus formed at high pheromone concentrations (usually when the mating parter is in a close proximity), fuse to form a diploid (Figure 1.1).

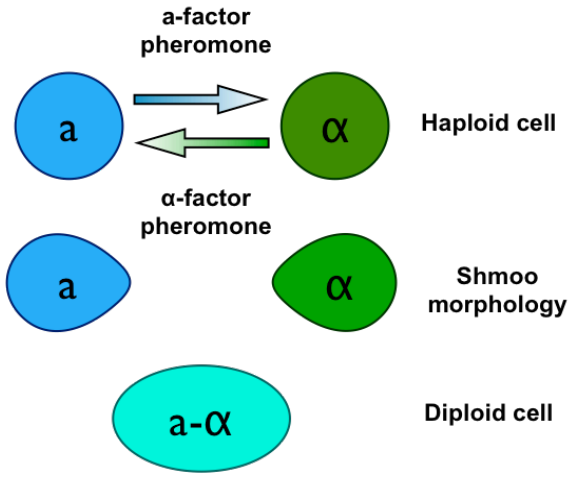

Figure 1.1: **Mating in yeast**. Yeast detect mating pheromone secreted by the opposite mating type and form mating projections that facilitate cell-cell fusion during mating.

A canonical signaling pathway, involving a G-protein coupled receptor (GPCR) and a mitogen activated protein kinase (MAPK) cascade (Figure 1.2) [15, 16, 17] regulates mating in yeast. The GPCR Ste2 is bound to a heterotrimeric G-protein comprised of an α- subunit, Gpa1 and a $\beta\gamma$-heterodimer, Ste4/Ste18. Gα binds GDP and GTP, whereas G$\beta\gamma$ binds effector proteins and triggers downstream signaling. Gα associates with the G$\beta\gamma$ heterodimer only when it is in the GDP-bound inactive state [18]. Upon binding to pheromone, Ste2 undergoes a conformational change and stimulates the Gα subunit to exchange GDP for GTP. Thus Ste2 acts as a Guanine nucleotide exchange factor (GEF) for Gα. GTP-bound active Gα dissociates

from the G$\beta\gamma$ heterodimer. Free G$\beta\gamma$ activates a downstream MAPK cascade leading to the expression of specific genes that induce physiological and morphological changes required for mating [19].

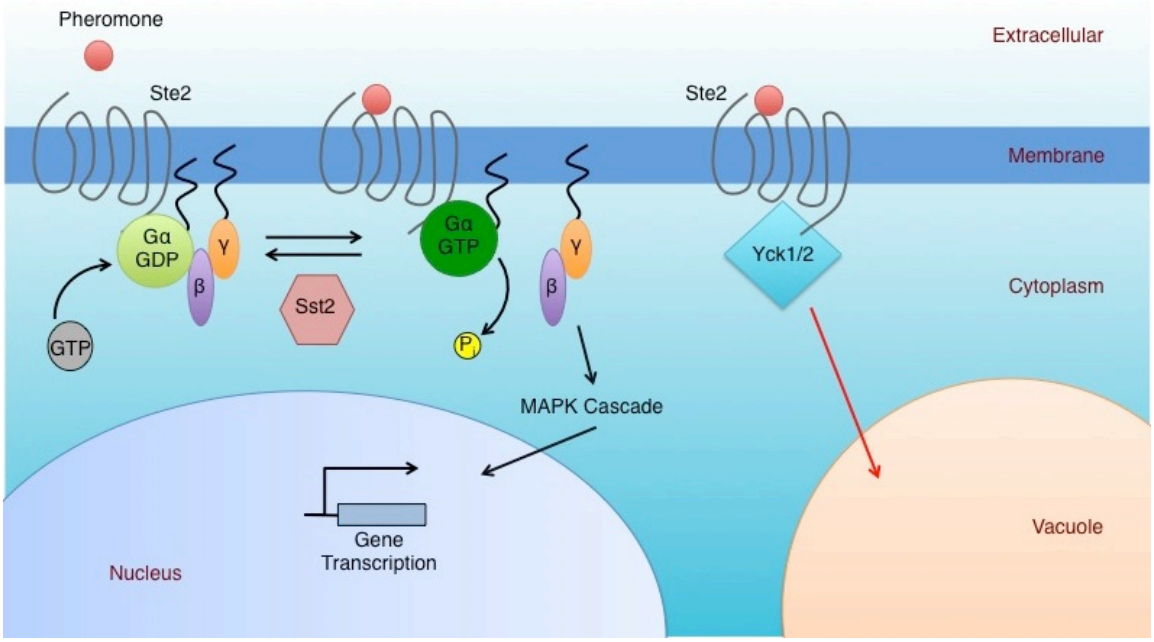

Figure 1.2: **Pheromone response pathway in yeast** . The mating pathway in yeast consists of a GPCR Ste2, G-protein subunits Gα and G$\beta\gamma$, MAPK cascade and the RGS protein Sst2. Upon binding pheromone, Ste2 undergoes a conformational change resulting in the activation of Gα. Active Gα releases G$\beta\gamma$, which in turn, results in the activation of a MAPK cascade culminating in the transcription of mating specific genes. Sst2 acts as a GTPase activating protein (GAP) by hydrolyzing GTP bound to Gα. Gα-GDP is inactive and it sequesters free G$\beta\gamma$, thereby, deactivating the mating pathway. Kinases Yck1/2 bind "active" Ste2 and phosphorylate the receptor. This leads to the ubiquination and internalization of the receptor. Ste2, upon internalization gets degraded in the vacuole.

Mating pathway activation also induces transcription of SST2, a gene that encodes the regulator of G- protein signaling (RGS protein) Sst2. Sst2 acts as a GTPase accelerating protein (GAP) for Gα, accelerating GTP hydrolysis [11, 20]. GDP-bound Gα rapidly reassociates with G$\beta\gamma$, terminating the response. Thus Sst2 plays a role in signal termination or pathway desensitization (Figure **??**). In addition to an RGS domain, which required for GAP activity, Sst2 posses a DEP domain through which it interacts with the GPCR Ste2 [21], suggesting

multiple roles for Sst2 in GPCR signaling.

1.2 Receptor polarization and pheromone-induced receptor endocytosis

Acting as a sensor for pheromone, Ste2 has an important role to play in gradient sensing [22, 23]. Ste2 is uniformly distributed over the cell surface in vegetative cells, but pheromone induces its polarization [24]. Ste2 polarization has been implicated for efficient gradient sensing by yeast [23] and is known to involve pheromone dependent receptor endocytosis. In theory, gradient sensing could occur through equilibrium binding and dissociation kinetics of pheromone and the receptor. However, the fact that yeast can detect very shallow pheromone gradients [13], suggests that other mechanisms for amplifying the pheromone gradient exist. Efficient gradient tracking requires Sst2 as cells lacking the RGS protein fail to form mating projections [25]. While Sst2 role in pathway desensitization has long been established, its role in gradient sensing remains unknown.

Endocytosis refers to the internalization of receptor/ligand or both from cell surface to an internal endocytic compartment. Ste2 undergoes endocytosis constitutively and pheromone treatment enhances the rate of internalization. Theoretical investigations have suggested that receptor endocytosis coupled with directed transport can generate polarity of membrane proteins [26, 27, 28, 29]. However, recent investigations have shown the formation of a stable Ste2 polar crescent in the absence of actin-mediated transport [23], suggesting other mechanisms are involved in the generation of a polarized receptor distribution. Following stimulation with pheromone, kinases Yck1/2 phosphorylate the cytoplasmic tail of Ste2 (Figure **??**); Ste2 is then ubiquitinated, internalized and degraded [30, 31, 32]. Regions of Yck1 phosphorylation of Ste2 on the plasma membrane was suggested to be mutually exclusive with the site of Sst2 localization [21, 23]. Since Sst2 binds Ste2 through its DEP domains [21] it is possible that Sst2 plays a role in inhibiting Ste2 phosphorylation and hence receptor endocytosis. Previous studies have suggested that RGS proteins inhibit GPCR internalization in neurons [33, 34]. Here we investigate the role of Sst2 in regulating receptor endocytosis and polarization during

mating in yeast.

1.3 Mechanistic Modeling

Mechanistic models are often used to describe dynamical systems. A dynamical system, by definition, is one in which different states of a process are defined and the changes in these states with time are described. A system of ordinary differential equations is typical used to describe dynamical systems in mechanistic modeling. The behavior of dynamical systems varies depending on the parameters used to describe the system. Mechanistic modeling of biological systems is based on the premise that a simple mathematical model representing the essential features of a biological phenomenon, when simulated using right set of parameters, can reproduce the experimental observations. Conversely, to explain certain experimental observations, one can create a simple mathematical model involving previously known or unknown components and test if the model can capture the essential behavior of the biological process. Mechanistic models are often complicated to develop due to unidentified parameters but the models that are well built using reliable parameter estimates have a tremendous prediction power and can greatly aid in simplifying, accelerating and informing experimental research. Thus identifying the right set of parameters that describe the experimental observations is a crucial step in building mechanistic models with predictive power. Robustness is a concept widely used in Systems Biology to determine the quality of a mathematical model. Robustness broadly means that certain functional behavior of a system doesn't change with perturbations in the system. For example, a robust model with respect to changes in parameters could mean that the behavior of the model is not impacted by perturbations in parameter values. The implications of model predictions are, hence, highly dependent on model robustness.

1.4 Thesis contributions

We devised an integrated approach involving mathematical modeling and live-cell imaging experiments to investigate the role of Sst2 in Ste2 internalization and polarization. Mathematical modeling serves the purpose of testing a hypothesis, generating alternative hypotheses and predicting the output of perturbations in a system. Models thus developed can be validated experimentally, and the experimental observations can further improve the model, thus accelerating the whole process. Yeast offers a wonderful platform where, theoretical perturbations can be made feasible for experimental validation, due to the availability of extensive genetic tools. Live-cell imaging has the advantage of monitoring single cells over the time course of an experiment. Microfluidic devices allow cells to be exposed to a well-controlled environment, and facilitate imaging and tracking of the cells trapped in the chamber. Furthermore, our microfluidic devices provide us with an additional function of generating and maintaining gradients of pheromone and also switching the direction of the gradient with time.

Our results demonstrate a novel role of the RGS protein in GPCR signaling in yeast. The experiments described in Chapter 2 show that Ste2 polarizes in wild type cells upon pheromone treatment. The size of the polar cap depends on the concentration of pheromone stimulus. Cells lacking Sst2 fail to establish a stable polarized Ste2 distribution at the growing edge during pheromone response. Results in Chapter 2 also show that GAP activity of Sst2 is not required for receptor polarization, suggesting novel function for Sst2 in pheromone-dependent receptor endocytosis and recovery at the plasma membrane.The canonical model for receptor endocytosis fails to explain the loss of Ste2 polarization in *sst2*Δ cells. To explain our experimental observations, we created a mathematical model and we fit our experimental data to the model to find the model parameters. The top scoring parameter sets fit the experimental data well. Disrupting the interaction between Ste2 and Sst2 results in a loss of Ste2 polarization. Our mathematical model predicts this positive role of Sst2 requires pheromone-induced expression of this protein. This prediction is confirmed experimentally.

Together, these data have established a novel positive role for Sst2 in yeast mating response. This work has contributed to a greater understanding of the interaction between RGS proteins and GPCRs in yeast, which can be extended to other mammalian systems since the G-protein signaling pathways are highly conserved between yeast and mammals (Chapter 3).

In Chapter 2, I performed all the live-cell imaging experiments, analyzed the fluorescence microscopy data, developed the mathematical model, fit experimental data to the model simulations and performed parameter estimation. Dr. Gauri Dixit and Dr. Matthew Pena provided the yeast strains used in the chapter.

CHAPTER 2

THE RGS PROTEIN SST2 REGULATES RECEPTOR DYNAMICS DURING THE MATING RESPONSE OF YEAST

2.1 Introduction

Haploid a-type yeast express G-protein coupled receptor Ste2 on their cell membrane, which acts as a sensor for extra-cellular mating pheromone $\alpha-$factor. Ste2 binds to pheromone and initiates the mating response by activating the pheromone response pathway. Furthermore, Ste2 undergoes constitutive turnover, a phenomenon known as endocytosis. Endocytosis is the uptake of extra-cellular or membrane bound molecules into specialized compartments in the cell interior. Internalized Ste2 is degraded in the vacuole and new protein synthesis occurs. Pheromone-induced endocytosis of Ste2 is faster than constitutive Ste2 endocytosis. It was suggested that Ste2 endocytosis might play a role in gradient sensing and orientation of polarized growth [29, 35].

Ste2 polarizes at the growing edge of the cell later during the pheromone response and Ste2 endocytosis was shown to be necessary for Ste2 polarization [23]. But the mechanisms that regulate Ste2 endocytosis and establish a polarized Ste2 distribution are not known. Receptor polarization can be established by a directed transport of secretory vesicles containing receptors to the growth site [36], but reports have shown the formation of a polarized Ste2 distribution in the absence of an actin-mediated directed transport, suggesting the involvement other mechanisms [23].

Sst2, a negative regulator in the pheromone pathway, binds the cytoplasmic tail of Ste2 and

the binding site of Sst2 overlaps with the binding site of kinases Yck1/2 that phosphorylate the receptor [21]. Sst2 co-localizes with the receptors at the shmoo tip during pheromone response.

Here, we set out to investigate the role of Sst2 in pheromone-dependent endocytosis of Ste2. When wild type cells are treated with pheromone, we show that Ste2 undergoes endocytosis and polarizes at the growing edge. Moreover, the length of the Ste2 polar cap depends on the concentration of the pheromone stimulus. We demonstrate that cells lacking Sst2 fail to establish stable Ste2 polarization. We also show that point mutants in which GAP activity of Sst2 is attenuated show an enhanced receptor polarization.

2.2 Results

2.2.1 Pheromone-dependent endocytosis and recovery of Ste2 is regulated by Sst2

To begin our investigations we monitored fluorescence intensity at the cell membrane over time in cells containing a Ste2-GFP fusion protein (Figure 2.1 A). Previously, it has been shown that following stimulation with high levels of pheromone, Ste2 undergoes endocytosis and then reemerges in a polarized fashion at the shmoo tip [24]. Consistent with these findings, we observed an initial loss membrane-bound Ste2-GFP when wild-type cells are treated with 150 nM of pheromone (Figure 2.1 B). After 40 min, receptor began to return to the membrane in a polarized fashion at the shmoo tip (Figures 2.1 A, B). At a lower dose of pheromone (10 nM), where cells undergo elongated growth, the total membrane-bound receptor pool did not show an initial decrease, but increased significantly over time (Figures 2.1 A, E). Furthermore, we observed that at this pheromone concentration, Ste2 still became polarized at the growing edge, but the distribution of receptor was significantly broader than at high doses. (Figure 2.1 G).

RGS proteins attenuate signaling by binding to the Gα subunit of heterotrimeric G-proteins and hydrolyzing GTP. Some RGS proteins, including Sst2, also have been shown to bind directly to GPCRs [37, 21]. In neurons, experimental data suggest both properties of RGS

proteins are involved in stabilizing receptors at the plasma membrane [38]. Therefore, we sought to investigate if Sst2 similarly regulates endocytosis during the mating response, and if so characterize the properties of this protein required for receptor stabilization. To this end, we monitored Ste2-GFP fluorescence in cells lacking Sst2 (*sst2*Δ) following pheromone treatment. Note that to allow a comparison between results from different experiments, we measured unstimulated Ste2 levels for all strains used in our investigations in a single experiment (Figure 2.1 D). These measurements were then used to scale all fluorescent time series relative to wildtype cells. This normalization accounts for differences in illumination and other day to day variation between experiments performed in our microfluidics chamber. In the *sst2*Δ strain receptor endocytosis occurred upon treatment with high pheromone (Figures 2.1 A, B). Interestingly, however, unlike wildtype cells receptors did not recover to the cell membrane at later times. Additionally, at low doses, the increase in Ste2 at the membrane was significantly diminished as compared to WT cells (Figures 2.1 A, E). These results demonstrate that Sst2 is required for proper recovery of the receptor to the plasma membrane following pheromone treatment.

2.2.2 Pheromone-induced gene expression is not sufficient for receptor recovery

Following internalization the receptor Ste2 is degraded in vacuoles [32]. However, GFP is highly resistant to proteolysis, and thus GFP fluorescence in the vacuole is a measure of cumulative Ste2 internalization. Therefore, by tracking whole cell Ste2-GFP fluorescence (internal and membrane bound), we can monitor Ste2 induction over time. Monitoring whole cell Ste2-GFP fluorescence in both wildtype and *sst2*Δ yeast revealed that total Ste2 levels increase in both cell types to roughly the amount following pheromone treatment at both high and low doses (Figures 2.1 C, F). These results demonstrate that pheromone-dependent receptor induction is not sufficient to maintain stable receptor polarization at the growing edge.

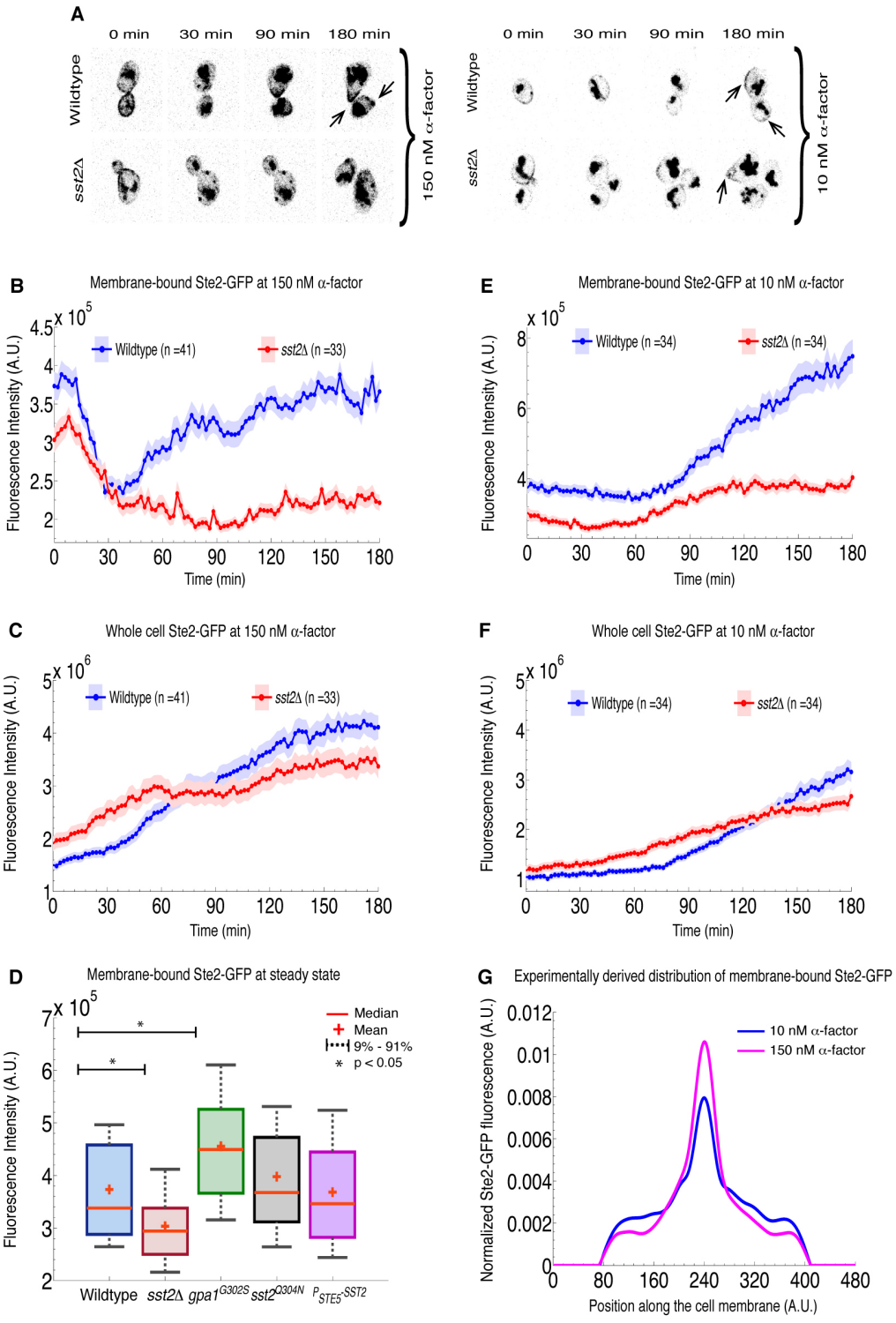
A
0 min
30 min
90 min
180 min
Wildtype
sst2Δ
150 nM α-factor
10 nM α-factor
B
Membrane-bound Ste2-GFP at 150 nM α-factor
Fluorescence Intensity (A.U.)
x 10^5
Wildtype (n =41)
sst2Δ (n =33)
Time (min)
E
Membrane-bound Ste2-GFP at 10 nM α-factor
Wildtype (n =34)
sst2Δ (n =34)
C
Whole cell Ste2-GFP at 150 nM α-factor
x 10^6
F
Whole cell Ste2-GFP at 10 nM α-factor
D
Membrane-bound Ste2-GFP at steady state
Median
Mean
9% - 91%
* p < 0.05
Wildtype
sst2Δ
gpa1G302S
sst2Q304N
PSTE5-SST2
G
Experimentally derived distribution of membrane-bound Ste2-GFP
Normalized Ste2-GFP fluorescence (A.U.)
10 nM α-factor
150 nM α-factor
Position along the cell membrane (A.U.)

2.2.3 Computational modeling predicts Sst2s role in regulating receptor endocytosis

To investigate the role of Sst2 in regulating receptor endocytosis, we developed a mathematical to describe signaling through the receptor Ste2 (Figure 2.2 C). The starting point for our investigations was the mathematical model of G-protein signaling in the yeast mating response developed by Yildirim et al [39]. In this model, pheromone binding stimulates the transition of the receptor Ste2 to active form Ste2*. The active receptor Ste2* is then phosphorylated ($Ste2*_p$), and the phosphorylated form of the receptor is available for internalization. Ste2* acts as GEF and facilitates the exchange of GDP to GTP on the Gα subunit Gpa1. GTP-bound Gpa1 (active form) dissociates from G$\beta\gamma$, resulting in free G$\beta\gamma$, which transduces the signal downstream resulting in increased expression of the receptor Ste2 (positive feedback) and the RGS protein Sst2 (negative feedback). In the model, the amount of

---

Figure 2.1: **Sst2 regulates pheromone-dependent endocytosis and recovery of the receptor**. A. Representative fluorescence microscopy images of Ste2-GFP in wildtype and *sst2*Δ cells treated with 150 nM and 10 nM pheromone. White arrows indicate receptor polarization. In cells that lack membrane bound receptors, cell boundary is shown in yellow. B. Ste2-GFP fluorescence on the membrane plotted against time in wildtype and *sst2*Δ cells. Solid lines represent the mean and light patches represent the standard error in the data. Cells were treated with 150 nM pheromone starting at 0min. C. Whole cell Ste2-GFP fluorescence in wild type and *sst2*Δ cells plotted against time. Solid lines represent the mean and light patches represent the standard error in the data. Cells were treated with 150 nM pheromone starting at 0min. D. Box plot of steady state Ste2-GFP fluorescence in untreated cells. Each box represents lower quartile (25%) - upper quartile (75%) of the data. Whiskers (dotted lines) represent values outside the upper and lower quartiles. Ends of the whiskers (solid black lines) represent 9th percentile and 91st percentile. Red bar represents the median of the data. + represents the mean of the data. E. Ste2-GFP fluorescence on the membrane plotted against time in wildtype and *sst2*Δ cells. Solid lines represent the mean and light patches represent the standard error in the data. Cells were treated with 10 nM pheromone starting at 0min. F. Whole cell Ste2-GFP fluorescence in wildtype and *sst2*Δ cells plotted against time. Solid lines represent the mean and light patches represent the standard error in the data. Cells were treated with 10 nM pheromone starting at 0min. G. Spatial distribution of Ste2-GFP in Wildtype cells shown by plotting normalized Ste2-GFP fluorescence profile on the membrane against the position on the cell. Each profile is centered at Ste2-GFP peak and the profiles are normalized such that the area under the curve is 1. Blue curve represents Ste2-GFP distribution in cells treated with 10nM pheromone. Magenta curve represents Ste2-GFP distribution in cells treated with 150nM pheromone.

free G$\beta\gamma$ determines the rate of gene induction. Sst2 acts as a GAP for the Gα subunit Gpa1. Upon GTP hydrolysis, Gpa1 reassociates with G$\beta\gamma$ forming inactive G-protein and turning off the pathway.

Using the normalized time series for wildtype and *sst2*Δ cells, we used a Monte Carlo method to perform parameter estimation and determine if the model could capture the behavior of both cell types (see Methods for details on parameter estimation). The model captured both endocytosis and recovery phases of the Ste2 dynamics in wildtype cells (Figure 2.2 A). However, it failed to capture the loss of Ste2 membrane recovery observed in *sst2*Δ cells (Figure 2.2 B), suggesting that unlike in neurons [38] Sst2s ability to accelerate GTPase activity is not sufficient to stabilize receptors at the membrane. The kinases Yck1/2 phosphorylate the cytoplasmic tail of the receptor Ste2. This leads to Ste2 being ubiquitinated, internalized and degraded. The binding site for Sst2 on Ste2 overlaps with the residues phosphorylated by Yck1/2, and it has been observed that phosphorylation of Ste2 displaces Sst2 [21]. Therefore, a potential mechanism that might explain our experimental observations is one in which Sst2 and Yck1/2 compete for access to Ste2. To test this mechanism, we updated our model to include Sst2s interaction with the receptor (Figure 2.2 C). In the revised model, the receptor can exist in three states: inactive (Ste2), active (Ste2*) and active and phosphorylated ($Ste2*_p$). Sst2 binds to both the inactive (Ste2) and active (Ste2*) forms of the receptor. Binding of Sst2 prevents the active form Ste2* from being phosphorylated. Ste2 and Ste2* are internalized at a basal rate which is 100-fold slower than the internalization rate of $Ste2*_p$. We again used Ste2-GFP fluorescence data from wild type and *sst2*Δ cells under high pheromone conditions to train the revised model. The revised model captured both the initial internalization and receptor recovery phases of wild type cells (Figure 2.2 D) and captured the loss of receptor recovery in *sst2*Δ cells (Figure 2.2 E). The details of the model are given in the following subsection.

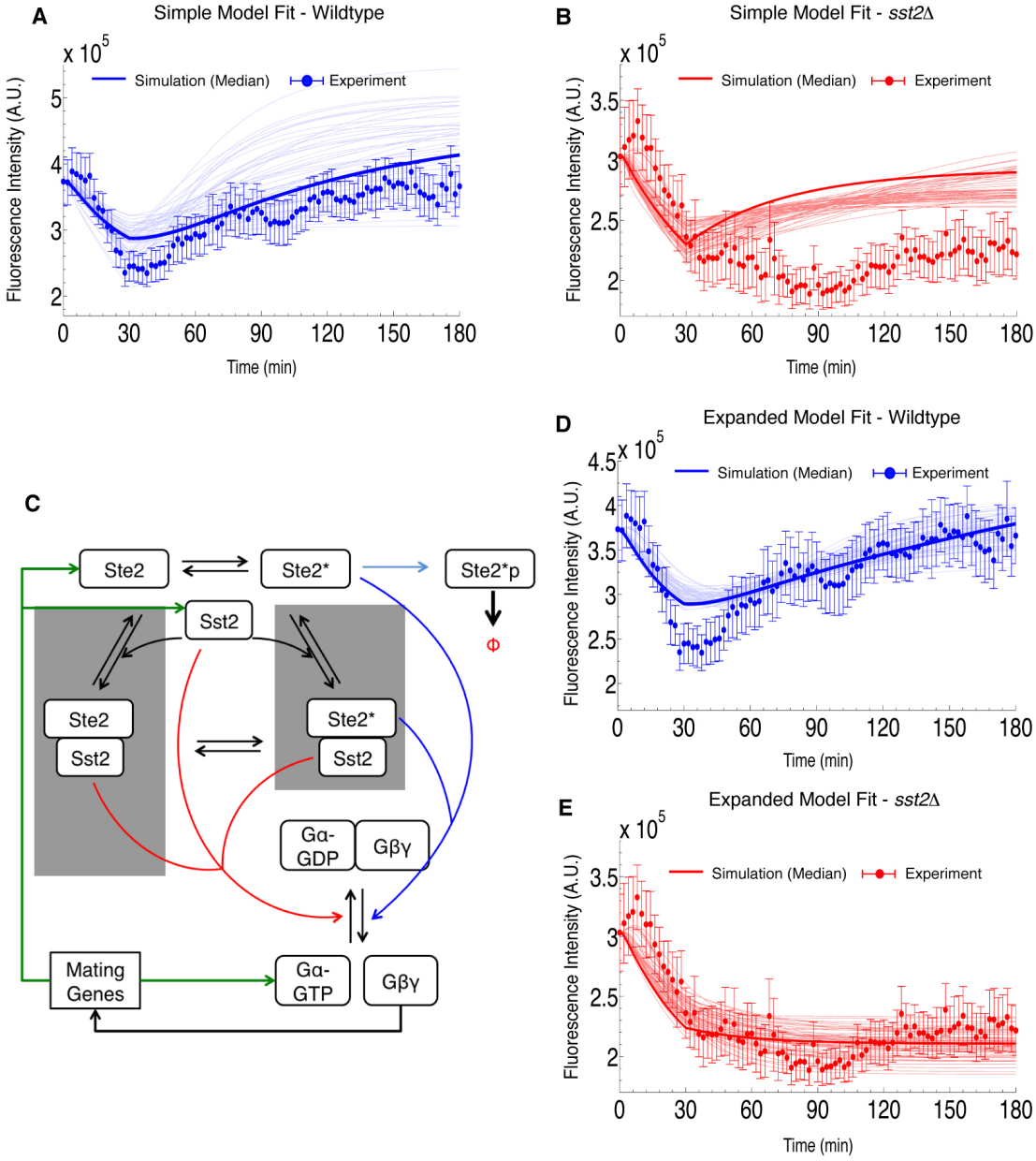
A
Simple Model Fit - Wildtype
x 10^5
Simulation (Median)
Experiment
Fluorescence Intensity (A.U.)
Time (min)
B
Simple Model Fit - sst2Δ
C
Ste2
Ste2*
Ste2*p
Φ
Sst2
Gα-GDP
Gβγ
Mating Genes
Gα-GTP
D
Expanded Model Fit - Wildtype
E
Expanded Model Fit - sst2Δ

2.2.4 Mathematical Model

The reaction network in the differential endocytosis model is shown in the figure 2.2 C.

Table 2.1 lists the species involved in the differential endocytosis model.

The differential endocytosis model can be described by the following set of ordinary differential equations.

The rate equation for free inactive Ste2

$$\frac{d[Ste2]}{dt} = k_1 + R_1 + R_2 + f_{IND} * (\frac{u_0[G\beta\gamma]^{hill_n}}{(K_0 + [G\beta\gamma]^{hill_n})} - k_5[Ste2]$$

Figure 2.2: **Computational modeling predicts Sst2s role in regulating receptor endocytosis**.
A. Ste2-GFP fluorescence data from wild type cells under high pheromone conditions was fit to the simple model simultaneously with experimental data from *sst2*Δ cells to estimate model parameters. Simulations using top 50 best fit parameter sets plotted in thin blue lines. Simulation using the median of top 50 best fit parameter sets plotted in bold blue line. Mean Ste2-GFP fluorescence along with 95% confidence intervals from experiments represented in blue circles with bars. B. Ste2-GFP fluorescence data from *sst2*Δ cells under high pheromone conditions was fit to the simple model simultaneously with experimental data from wild type cells to estimate model parameters. Simulations using top 50 best fit parameter sets plotted in thin red lines. Simulation using the median of top 50 best fit parameter sets plotted in bold red line. Mean Ste2-GFP fluorescence along with 95% confidence intervals from experiments represented in red circles with bars. C. Reaction network representing the expanded model. Reaction modules shaded in grey were added to the simple model to generate the expanded model. One sided black arrows represent irreversible reactions. Double-sided black arrows represent reversible reactions. Blue arrows represent GEF activity of the receptor. Red arrows represent GAP activity of Sst2. Green arrows represent gene induction/pheromone dependent synthesis. Bold black arrow represents endocytosis of phosphorylated receptor. D. Ste2-GFP fluorescence data from wild type cells under high pheromone conditions was fit to the expanded model simultaneously with experimental data from *sst2*Δ cells to estimate model parameters. Simulations using top 50 best fit parameter sets plotted in thin blue lines. Simulation using the median of top 50 best fit parameter sets plotted in bold blue line. Mean Ste2-GFP fluorescence along with 95% confidence intervals from experiments represented in blue circles with bars. E. Ste2-GFP fluorescence data from *sst2*Δ cells under high pheromone conditions was fit to the expanded model simultaneously with experimental data from wild type cells to estimate model parameters. Simulations using top 50 best fit parameter sets plotted in thin red lines. Simulation using the median of top 50 best fit parameter sets plotted in bold red line. Mean Ste2-GFP fluorescence along with 95% confidence intervals from experiments represented in red circles with bars.

Table 2.1:

List of species in the differential endocytosis model

Species name	**Description**
$[Ste2]$	Concentration of free inactive Ste2
$[Ste2*]$	Concentration of free active Ste2
$[G]$	Concentration of free inactive G-protein
$[G\alpha_{GDP}]$	Concentration of free inactive Gα
$[G\beta\gamma]$	Concentration of free G$\beta\gamma$
$[Sst2]$	Concentration of free Sst2
$[Ste2 - Sst2]$	Concentration of free inactive Ste2 bound to Sst2
$[Ste2 * -Sst2]$	Concentration of free active Ste2 bound to Sst2
$[Ste2_p]$	Concentration of free phosphorylated Ste2

The rate equation for free active Ste2 (bound to pheromone)

$$\frac{d[Ste2*]}{dt} = -R_1 + R_3 - \frac{u_5[Ste2*]}{(K_5 + [Ste2*])}$$

The rate equation for free G-protein

$$\frac{d[G]}{dt} = R_5 - R_4$$

The rate equation for free $G\alpha_{GDP}$

$$\frac{d[G\alpha_{GDP}]}{dt} = syn_{G\alpha} + R_6 - R_5 + f_{IND} * \frac{u_1[G\beta\gamma]}{(K_1 + [G\beta\gamma])} - k_{14}[G\alpha_{GDP}]$$

The rate equation for free $G\beta\gamma$

$$\frac{d[G\beta\gamma]}{dt} = syn_{G\beta\gamma} + R_4 - R_5 + f_{IND} * \frac{u_2[G\beta\gamma]}{(K_2 + [G\beta\gamma])} - k_15[G\beta\gamma]$$

The rate equation for free Sst2

$$\frac{d[Sst2]}{dt} = syn_{Sst2} + R_2 + R_3 + f_{IND} * \frac{u_3[G\beta\gamma]}{(K_3 + [G\beta\gamma])} - (k_{10} + k_{11}[G\beta\gamma])[Sst2]$$

The rate equation for $FUS1_{LacZ}$

$$\frac{d[Fus1_{LacZ}]}{dt} = \frac{u_4[G\beta\gamma]}{(K_4 + [G\beta\gamma])} - k_{12}[Fus1_{LacZ}]$$

The rate equation for free Ste2-Sst2 complex

$$\frac{d[Ste2 - Sst2]}{dt} = -R_2 + R_7 - k_5[Ste2 - Sst2]$$

The rate equation for free Ste2*-Sst2 complex

$$\frac{d[Ste2* - Sst2]}{dt} = -R_3 + R_7 - k_5[Ste2* - Sst2]$$

The rate equation for free phosphorylated Ste2 ($Ste2_P$)

$$\frac{d[Ste2_P]}{dt} = \frac{u_5[Ste2*]}{(K_5 + [Ste2*])} - k_4[Ste2_P]$$

where [A] represents the concentration of the species A.

The reaction fluxes R_is are defined as follows:

$$R_1 = k_3[Ste2*] - k_2[Ste2][L]$$

describes the formation and dissociation of active Ste2 (bound to pheromone)

$$R_2 = k_{17}[Ste2 - Sst2] - k_{16}[Ste2][Sst2]$$

describes the formation and dissociation of Ste2-Sst2 complexes

$$R_3 = k_{17}[Ste2* - Sst2] - k_{16}[Ste2*][Sst2]$$

describes the formation and dissociation of active Ste2-Sst2 complexes

$$R_4 = (k_6[Ste2*] + k_{6\prime\prime}[Ste2 * -Sst2] + k_{6\prime})[G]$$

describes the activation of G-protein

$$R_5 = k_7[G\beta\gamma][G\alpha_{GDP}]$$

describes the inactivation of G-protein

$$R_6 = (k_8[Ste2 - Sst2] + k_8[Ste2 * -Sst2] + k_{8\prime}[Sst2] + k_9)[G\beta\gamma]$$

describes the hydrolysis of $G\alpha - GTP$ to $G\alpha - GDP$

$$R_7 = k_3[Ste2 * -Sst2] - k_2[Ste2 - Sst2][L]$$

describes the formation and dissociation of active Ste2 (bound to pheromone) that is already bound to Sst2.

Table 2.2 lists the parameters in the differential endocytosis model and the median values of each parameter from top 50 parameters sets obtained by parameter estimation.

2.2.5 Model Robustness

Robustness analysis was performed to test the sensitivity of the model to perturbations in the parameters (See Methods). Robustness of the model to perturbations in parameters was estimated by calculating the coefficient of variation of each parameter in the best 50 parameter sets.

Table 2.3 lists the coefficient of variation (CV) of all parameters within the top 50 parameters sets obtained by parameter estimation.

Table 2.2:

List of parameters in the differential endocytosis model

Parameter	Description	Value	Units	Source
k_4	Pheromone-induced receptor endocytosis rate	0.0436	s^{-1}	
$k_{6\prime}$	Constitutive G-protein activation rate	$7.1748 * 10^{-7}$	$molec^{-1}s^{-1}$	
$k_{6\prime\prime}$	GEF activity of active receptor bound to Sst2	$2.9115 * 10^{-5}$	s^{-1}	
k_6	GEF activity of active receptor	$5.4946 * 10^{-6}$	s^{-1}	
k_7	G-protein deactivation rate	$5.7684 * 10^{-4}$	$molec^{-1}s^{-1}$	
k_8	GAP activity of Sst2 bound to Ste2	$7.6511*^{-5}$	$molec^{-1}s^{-1}$	
u_0	Maximum Ste2 synthesis rate	0.4576	$molecs^{-1}$	
u_1	Maximum $G\alpha_{GDP}$ synthesis rate	6.0478	$molecs^{-1}$	
u_2	Maximum $G\beta\gamma$ synthesis rate	6.7333	$molecs^{-1}$	
u_3	Maximum Sst2 synthesis rate	5.7568	$molecs^{-1}$	
u_4	Maximum $Fus1_{LacZ}$ synthesis rate	51.1867	$molecs^{-1}$	
u_5	Maximum receptor phosphorylation rate	7.7019	$molecs^{-1}$	
K_0	Michaelis constant for Ste2 synthesis	471.6257	$molec$	
K_1	Michaelis constant for $G\alpha_{GDP}$ synthesis	$4.1852 * 10^3$	$molec$	
K_2	Michaelis constant for $G\beta\gamma$ synthesis	$4.0342 * 10^3$	$molec$	
K_3	Michaelis constant for Sst2 synthesis	$6.222 * e^3$	$molec$	
K_4	Michaelis constant for $Fus1_{LacZ}$ synthesis	$5.544 * 10^4$	$molec$	
K_5	Michaelis constant for receptor phosphorylation	$4.1256 * 10^3$	$molec$	
k_{11}	Pheromone induced degradation rate of Sst2	$5.6154 * 10^{-8}$	$molec^{-1}s^{-1}$	
k_{12}	$Fus1_{LacZ}$ degradation rate constant	$4.5463 * 10^{-6}$	s^{-1}	
k_{14}	$G\alpha_{GDP}$ degradation rate constant	$2.4416 * 10^{-4}$	s^{-1}	
k_{15}	$G\beta\gamma$ degradation rate	$3.1825 * 10^{-4}$	s^{-1}	
k_{16}	Ste2 and Sst2 association rate	376.6992	$M^{-1}s^{-1}$	
k_{17}	Ste2 and Sst2 dissociation rate	0.0053	s^{-1}	
$syn_{G\beta\gamma}$	$G\beta\gamma$ constitutive synthesis rate	$4.0733 * 10^{-5}$	$molecs^{-1}$	
$syn_{G\alpha}$	$G\alpha_{GDP}$ constitutive synthesis rate	0.4952	$molecs^{-1}$	
a	Sst2-dependent GTP hydrolysis rate	3.4869	$-$	
b		44.5793	$-$	
$hill_n$	Hill coefficient for pheromone induced receptor synthesis	2.7497	$-$	
k_1	Receptor constitutive synthesis rate	4	$molecs^{-1}$	[39]
k_2	Pheromone receptor association rate	$1.067 * 10^3$	$M^{-1}s^{-1}$	[39]
k_3	Pheromone receptor dissociation rate	$1.1 * 10^{-3}$	s^{-1}	[39]
k_5	Constitutive receptor endocytosis rate	$5 * 10^{-4}$	s^{-1}	[39]
k_9	Constitutive GTP hydrolysis rate	$4 * 10^{-3}$	s^{-1}	[40]
k_{10}	Degradation rate of Sst2	$8 * 10^{-4}$	s^{-1}	[39]
syn_{Sst2}	Sst2 constitutive synthesis rate	1.6	$molecs^{-1}$	[39]

Table 2.3:

Sensitivity of parameters

Parameter	CV	Parameter	CV	Parameter	CV
k_4	0.7418	u_4	0.5844	k_{12}	0.6236
$k_{6\prime}$	0.4686	u_5	0.1723	k_{14}	0.7873
$k_{6\prime\prime}$	0.6652	K_0	0.6132	k_{15}	0.6677
k_6	0.4362	K_1	0.5592	k_{16}	0.5918
k_7	0.5530	K_2	0.7242	k_{17}	0.4546
k_8	0.4197	K_3	0.4398	$syn_{G\beta\gamma}$	0.6262
u_0	1.5758	K_4	0.5680	$syn_{G\alpha}$	0.5037
u_1	0.5919	K_5	0.3213	a	0.6514
u_2	0.3351	k_{11}	0.4054	$hill_n$	0.9607
u_3	0.3868	b	0.6535		

u_5, which is the maximum receptor phosphorylation rate (Figure 2.3 A) is the most highly constrained parameter in the model (CV = 0.1723). The model was also sensitive to the michaelis constant (K_5) for receptor phosphorylation (CV = 0.3213) (Figure 2.3 B). The sensitivity of the model to parameters related to receptor phosphorylation is logical as the competition between Sst2 and the phosphorylation machinery in binding to the receptor is the main component in the model. However, the model was highly robust for rest of the parameters including Sst2-Ste2 binding and Ste2 internalization (Figures 2.4-2.8).

2.2.6 Loss of GAP activity of Sst2 enhances receptor polarization

A prediction of the model is that GAP activity is not required to stabilize receptor at the membrane. To test this prediction, we used the point mutant *gpa1*^{G302S} that prevents the Gα subunit from interacting with Sst2 and, therefore, prevents Sst2 from acting as a GAP [21]. Consistent with the model, the *gpa1*^{G302S} mutant did not exhibit the defect in receptor recovery seen in the *sst2*Δ strain, but rather showed increased membrane-bound receptor in comparison to wildtype cells (Figures 2.9 A, B, C). Note that Ste2-GFP fluorescence data was normalized so that Ste2-GFP values in wild type and *gpa1*^{G302S} cells at t=0minmatch the respective Ste2-GFP fluorescence at steady state (Figure 2.1 D). Whole cell Ste2-GFP fluorescence in the *gpa1*^{G302S} mutant reached a similar level as wildtype cells (Fig 2C), demonstrating that

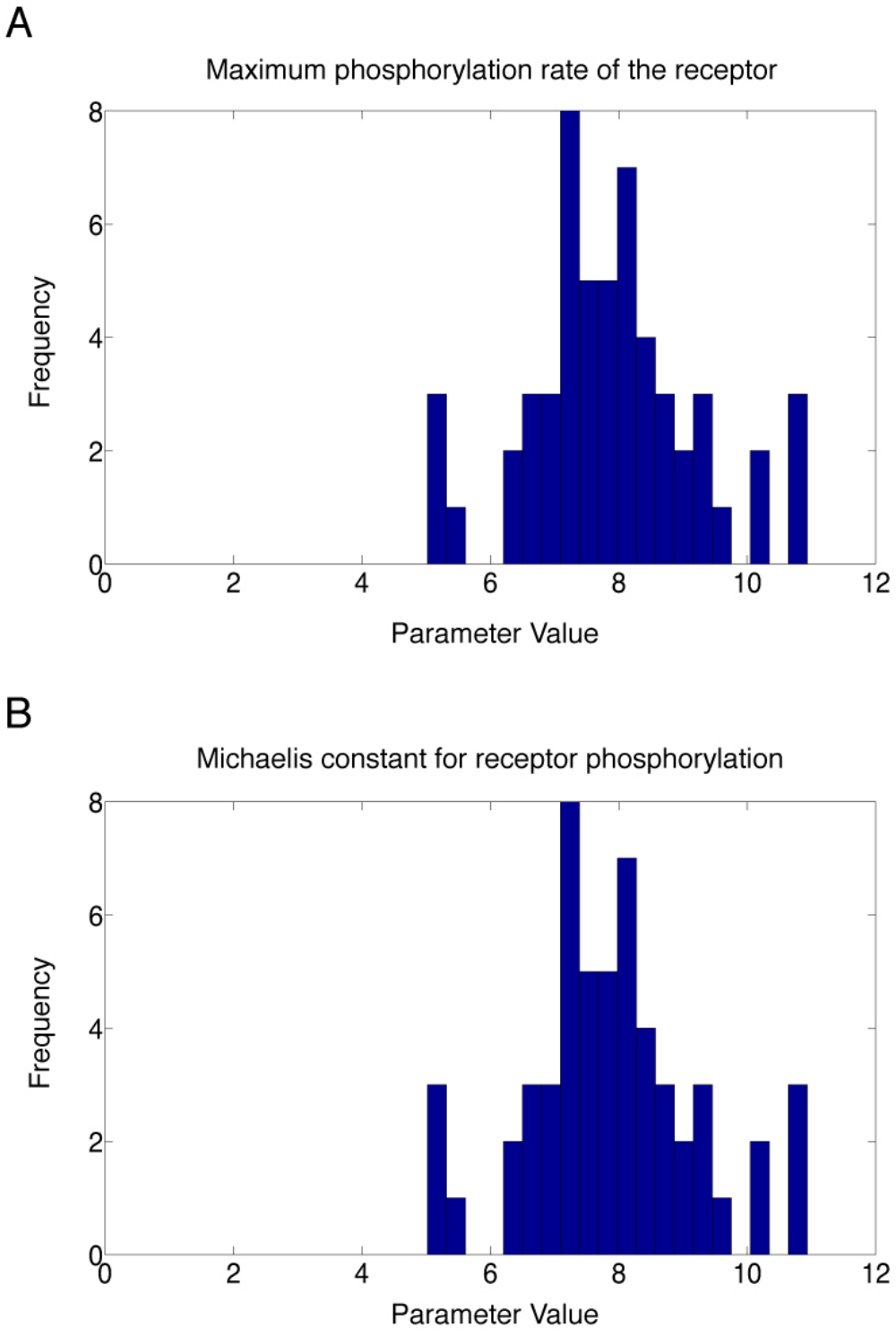

Figure 2.3: **Histograms of sensitive parameters in the differential endocytosis model**. A. Maximum phosphorylation rate of the receptor (CV = 0.1723) B. Michaelis constant for the phosphorylation of the receptor (CV = 0.3213)

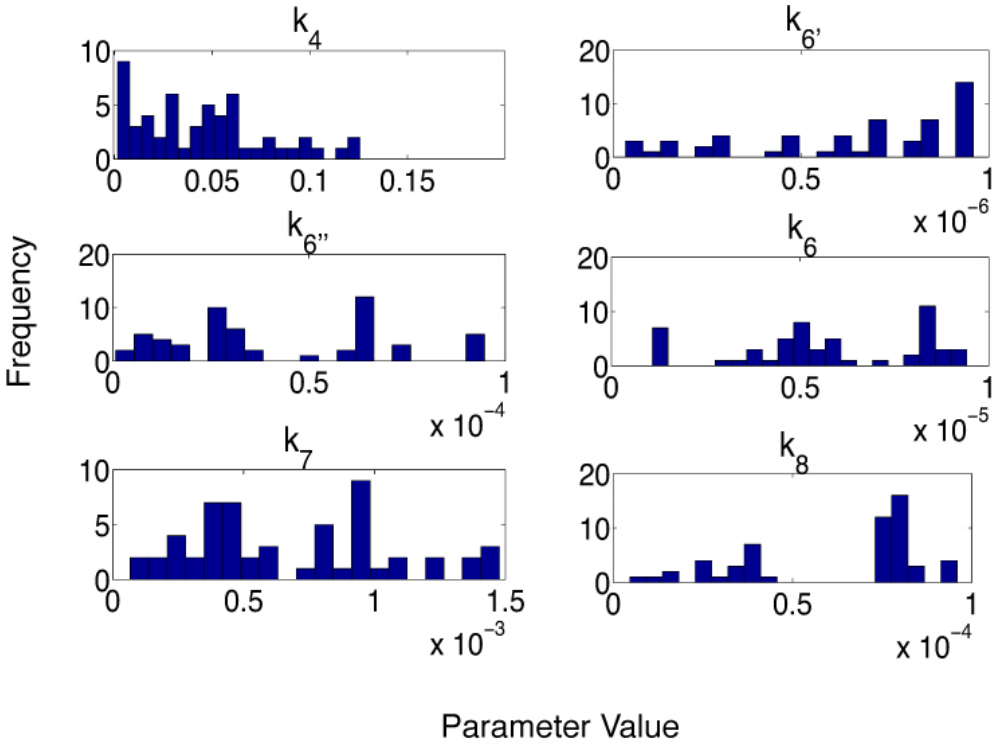

Figure 2.4: **Histograms of parameters in the differential endocytosis model**.

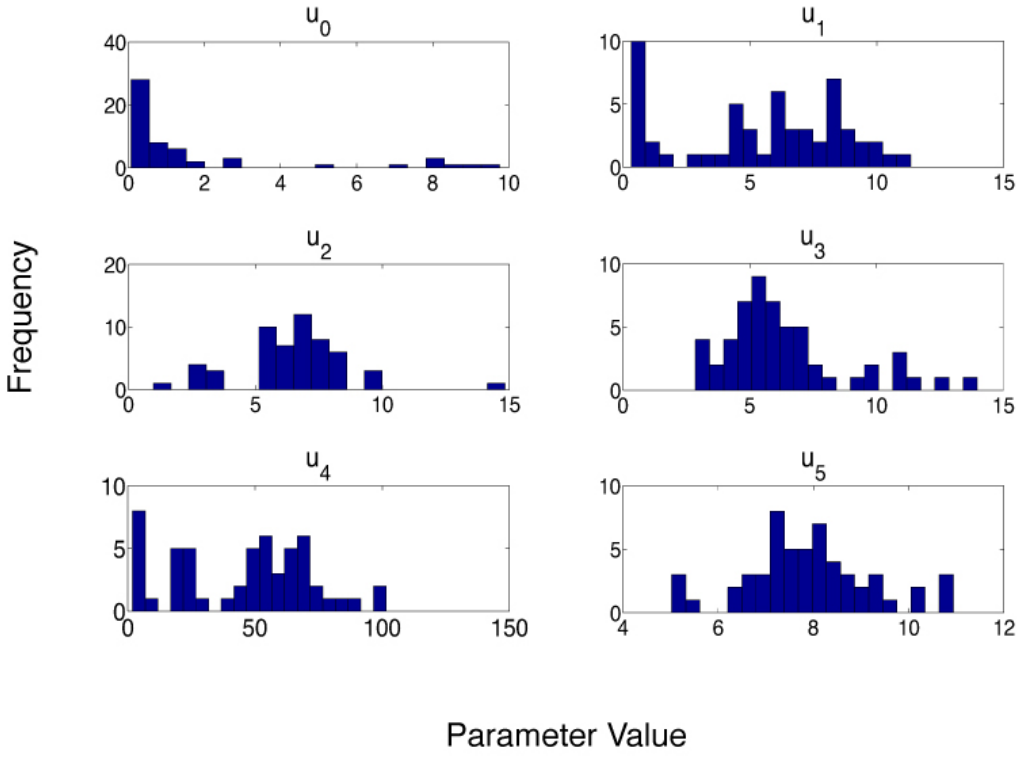

Figure 2.5: **Histograms of parameters in the differential endocytosis model**.

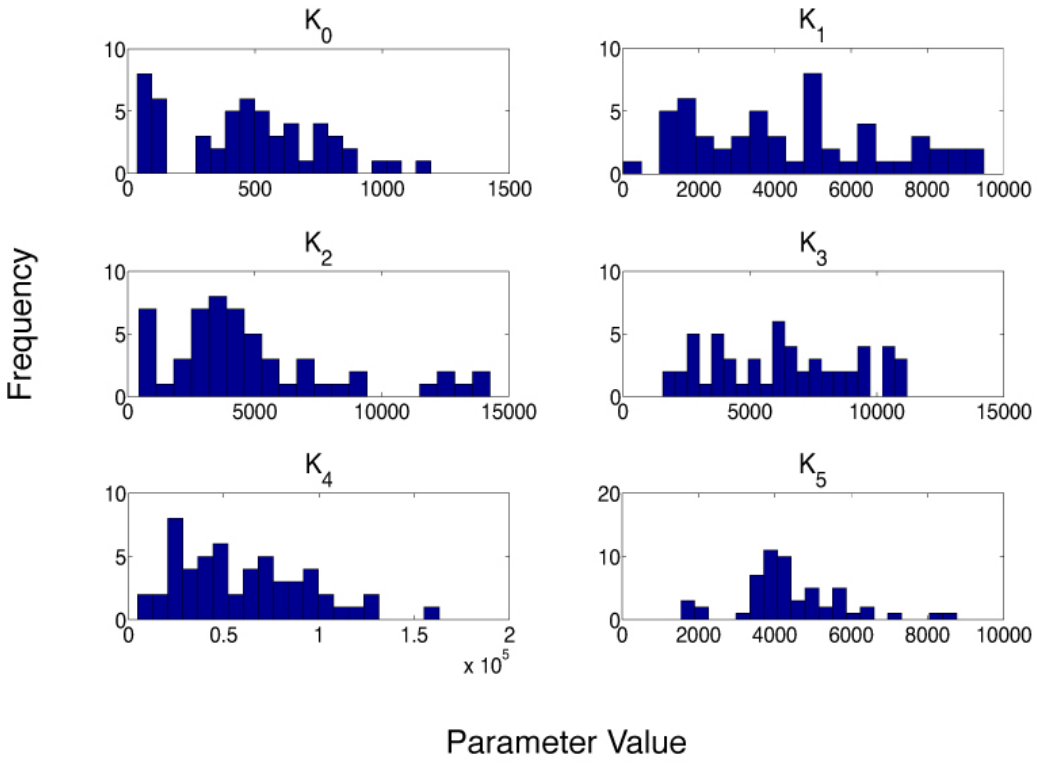

Figure 2.6: **Histograms of parameters in the differential endocytosis model**.

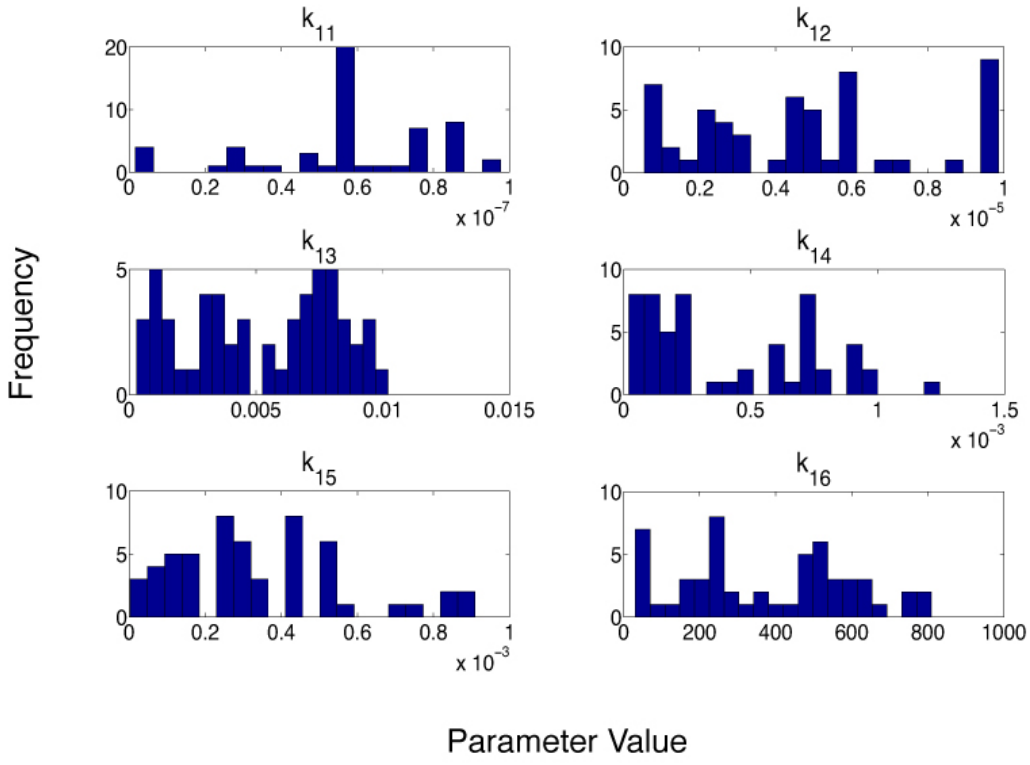

Figure 2.7: **Histograms of parameters in the differential endocytosis model**.

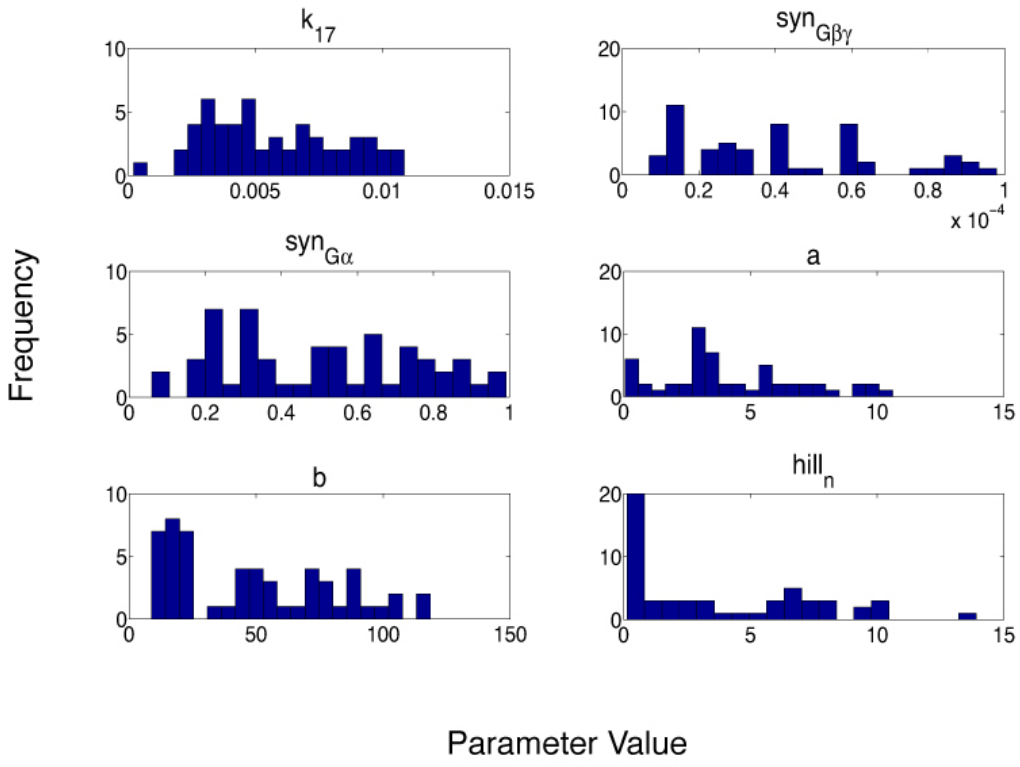

Figure 2.8: **Histograms of parameters in the differential endocytosis model**.

increased receptor expression was not responsible for receptor recovery in this strain. Furthermore, the distribution of the receptor on the plasma membrane was broader in $gpa1^{G302S}$ mutant as compared to the wild type cells (Figures 2.10 B).

2.2.7 Sst2s interaction with Ste2 is required to stabilize the receptor at the membrane

To test the model prediction that Sst2s interaction with Ste2 is necessary for receptor recovery we used the point mutant $sst2^{Q304N}$ that disrupts the interaction between Sst2 and Ste2 [21]. Our model predicts that in these cells recovery should not occur (Figure 2.9 D). In agreement with this prediction and similar to $sst2\Delta$ cells, this strain did not show any recovery of the receptor (Figure 2.10 A, E). Note that Ste2-GFP fluorescence data was normalized so that Ste2-GFP values in wild type and $sst2^{Q304N}$ cells at t=0minmatch the respective Ste2-GFP fluorescence at steady state (Figure 2.1 D).

2.2.8 Sst2 induction is necessary for Ste2 polarization

Sst2 is induced in response to pheromone, and it is typically assumed that this increase in Sst2 levels forms a negative feedback loop that leads to signal attenuation. Interestingly, our model predicts that pheromone-dependent induction of Sst2 is necessary for receptor recovery (Figure 2.10 F). To test this prediction we expressed SST2 under a non-inducible promoter. In particular, we replaced the endogenous promoter of SST2 with STE5 promoter, which is not responsive to pheromone. With this promoter, the steady state abundance of Ste2 on the membrane is comparable to wildtype yeast (Fig 5F). Consistent with our model, when treated with 150 nM pheromone, cells containing P_{STE5}-*SST2* showed less recovery compared to the wildtype strain (Figures 2.10 A, G). Note that Ste2-GFP fluorescence data was normalized so that Ste2-GFP values in wild type and P_{STE5}-*SST2* cells at t=0minmatch the respective Ste2-GFP fluorescence at steady state (Figure 2.1 D).

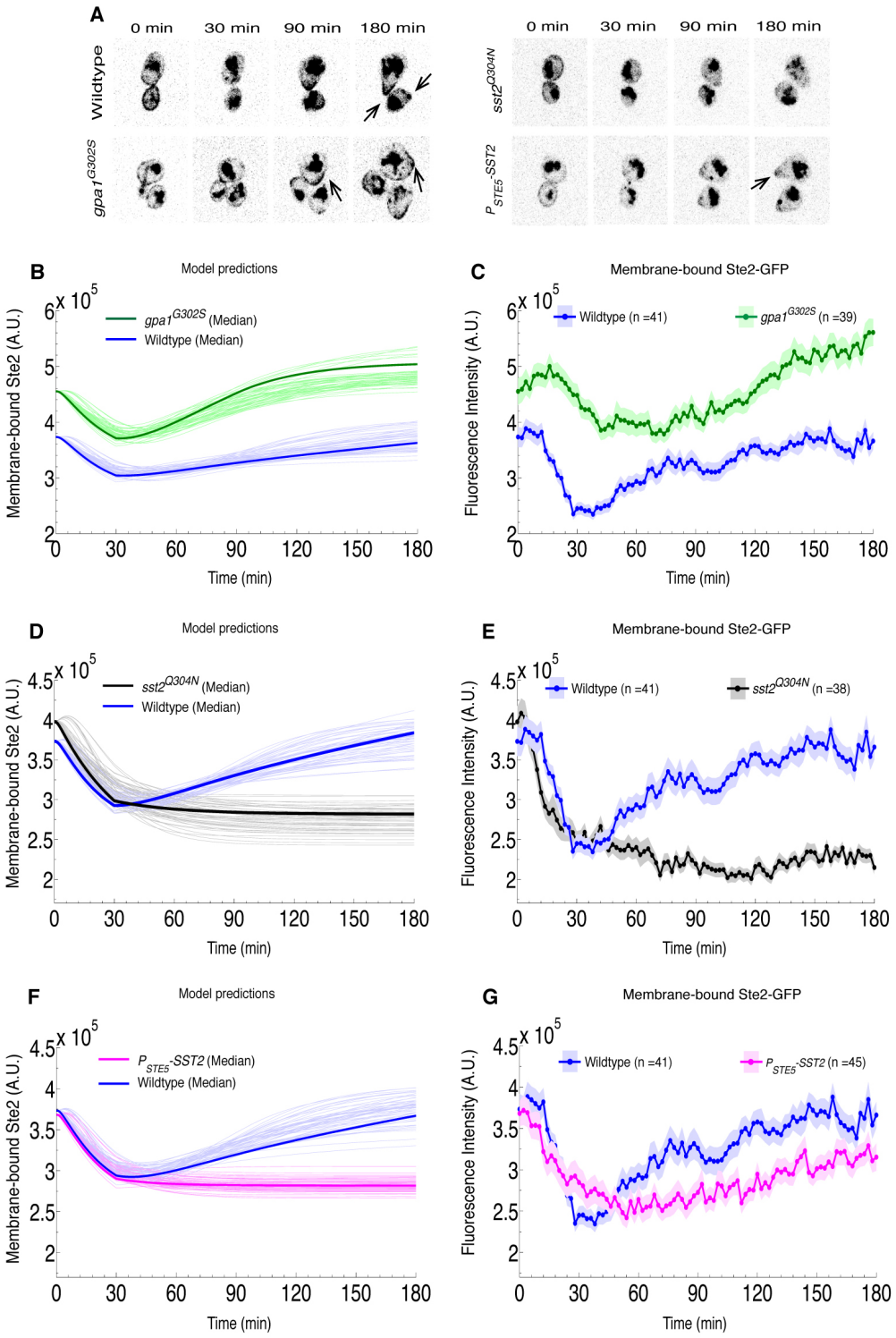
A
0 min
30 min
90 min
180 min
Wildtype
gpa1G302S
sst2Q304N
PSTE5-SST2
B
Model predictions
x 10^5
gpa1G302S (Median)
Wildtype (Median)
Membrane-bound Ste2 (A.U.)
Time (min)
C
Membrane-bound Ste2-GFP
Wildtype (n =41)
gpa1G302S (n =39)
Fluorescence Intensity (A.U.)
Time (min)
D
Model predictions
sst2Q304N (Median)
Wildtype (Median)
Membrane-bound Ste2 (A.U.)
Time (min)
E
Membrane-bound Ste2-GFP
Wildtype (n =41)
sst2Q304N (n =38)
Fluorescence Intensity (A.U.)
Time (min)
F
Model predictions
PSTE5-SST2 (Median)
Wildtype (Median)
Membrane-bound Ste2 (A.U.)
Time (min)
G
Membrane-bound Ste2-GFP
Wildtype (n =41)
PSTE5-SST2 (n =45)
Fluorescence Intensity (A.U.)
Time (min)

Figure 2.9: **Sst2-Ste2 binding and Sst2 induction, but not Sst2 GAP activity, is necessary for pheromone dependent receptor recovery**.
A. Representative fluorescence microscopy images of Ste2-GFP in wildtype, $gpa1^{G302S}$, $sst2^{Q304N}$ and P_{STE5}-*SST2* cells treated with 150 nM pheromone. White arrows indicate the presence of receptor polarization at the growth site. B. Model prediction for Ste2-GFP on the cell membrane in wild type cells shown in blue. Individual predictions using top 50 parameter sets shown in thin blue lines. Simulation using the median of the top 50 parameter sets is shown in dark blue line. Model prediction for Ste2-GFP on the cell membrane in $gpa1^{G302S}$ cells shown in green. Individual predictions shown in thin green lines and simulation using the median of the top 50 parameter sets is shown in solid green line. Simulations were performed under high pheromone conditions. C. Ste2-GFP fluorescence on the membrane from live cell imaging plotted against time. Wildtype data shown in blue. Solid blue line represents the mean and light blue patch shows standard error in the data. $gpa1^{G302S}$ data is shown in green. Solid green line represents the mean and light green patch shows standard error in the data. Cells were treated with 150 nM pheromone starting at 0min. D. Model prediction for Ste2-GFP on the cell membrane in wild type cells shown in blue. Individual predictions using top 50 parameter sets shown in thin blue lines. Simulation using the median of the top 50 parameter sets is shown in dark blue line. Model prediction for Ste2-GFP on the cell membrane in $sst2^{Q304N}$ cells shown in black. Individual predictions shown in thin grey lines and simulation using the median of the top 50 parameter sets is shown in solid black line. Simulations were performed under high pheromone conditions. E. Ste2-GFP fluorescence on the membrane from live cell imaging plotted against time. Wildtype data shown in blue. Solid blue line represents the mean and light blue patch shows standard error in the data.$sst2^{Q304N}$ data is shown in black. Solid black line represents the mean and light grey patch shows standard error in the data. Cells were treated with 150 nM pheromone starting at 0min. F. Model prediction for Ste2-GFP on the cell membrane in wild type cells shown in blue. Individual predictions using top 50 parameter sets shown in thin blue lines. Simulation using the median of the top 50 parameter sets is shown in dark blue line. Model prediction for Ste2-GFP on the cell membrane in P_{STE5}-*SST2* cells shown in magenta. Individual predictions shown in thin magenta lines and simulation using the median of the top 50 parameter sets is shown in solid magenta line. Simulations were performed under high pheromone conditions. G. Ste2-GFP fluorescence on the membrane from live cell imaging plotted against time. Wildtype data shown in blue. Solid blue line represents the mean and light blue patch shows standard error in the data. P_{STE5}-*SST2* data is shown in magenta. Solid magenta line represents the mean and light magenta patch shows standard error in the data. Cells were treated with 150 nM pheromone starting at 0min.

2.2.9 Sst2 plays a role in establishing a polarized Ste2 distribution

Our Ste2 internalization data revealed that Sst2 regulates receptor endocytosis and stabilizes the receptor on the plasma membrane. Because receptor endocytosis was previously shown to be important for receptor polarization [23], we sought to investigate the effect of Sst2 on Ste2 distribution on the plasma membrane. We quantified receptor polarization using Ste2-GFP fluorescence data. The extent of Ste2 polarization was measured using a Polarization Index metric, as explained below.

Polarization Index measures the shift in the center of mass of a cell due to a polarized protein distribution. Polarization Index of membrane Ste2 (PI_{STE2}) in a yeast cell at a particular time point was calculated from the Ste2-GFP fluorescent images as follows:

$$PI_{STE2} = \frac{d_{GC-CoM}}{r_{eff}} \tag{2.1}$$

$d_{GC\text{-}CoM}$ is the distance between geometric center (GC) of a cell and the Center of Mass (CoM) of Ste2 in that particular cell.

If X and Y represent a set of N coordinates (x_i, y_i), i=1,2,3,N of pixels of the cell membrane,

$$GC = \left(\frac{\sum_{i=1}^{N} x_i}{N}, \frac{\sum_{i=1}^{N} y_i}{N} \right)$$

And let I_{xy} represent the intensity of Ste2 in a pixel at a coordinate (x, y).

$$CoMofSte2 = \left(\frac{\sum_{i=1}^{N} x_i * I_{x_i y_i}}{N}, \frac{\sum_{i=1}^{N} y_i * I_{x_i y_i}}{N} \right)$$

r_{eff} is the effective radius of the cell. r_{eff} is equal to r (radius of the cell) if the yeast cell is circular. Otherwise,

$$r_{eff} = \sqrt{\frac{A}{\pi}},$$

where A is the area of the cell.

PI can range from 0 (uniform distribution) to 1 (highly polarized distribution)

Since Polarization Index metric depends on center of mass of protein distribution, a broad polar cap can often times have same polarization index as a highly concentrated puncta such as an endosome near the plasma membrane. To normalize the bias created due to center of mass, the polarization index was plotted against the mean Ste2-GFP intensity on the front half of the cell. The amount of Ste2 in the front half of the cell was calculated by converting the Ste2-GFP fluorescence data into polar coordinates. Ste2-GFP peak in each cell was aligned to $\theta = 0$ and the fluorescence intensity of Ste2-GFP between $\theta = \frac{\pi}{2}$ and $\theta = \frac{\pi}{2}$ was measured to give the amount of Ste2-GFP in the front half of the cell.

At high pheromone, wild type cells show strong polarization and have high receptor in the front half. *sst2*Δ cells have a high Ste2 polarization index but they have low receptor abundance on the front half of the cell (Figures 2.10 A). Ste2-GFP abundance in the front half of *gpa1*^{G302S} is similar to that of wild type, but these cells have low polarization index. *gpa1*^{G302S} cells form a broad Ste2-GFP cap instead of Ste2-GFP tightly localized at the shmoo tip (Fig 6B). Hence the low polarization index despite high receptor abundance. *sst2*^{Q304N} shows weak polarization and has low receptor abundance under high pheromone conditions (Fig 6A). At low pheromone, wild type cells have high receptor abundance but have a low polarization index as the cells are not polarized (they undergo budding and form a broad Ste2-GFP cap). *sst2*Δ cells on the other hand are strongly polarized but have the lowest receptor abundance compared to other strains. *gpa1*^{G302S} has the highest receptor abundance and shows

strong polarization under these conditions. *sst2*^{Q304N} though has lower receptor abundance than wild type, shows significant polarization at low pheromone conditions (Fig S2).

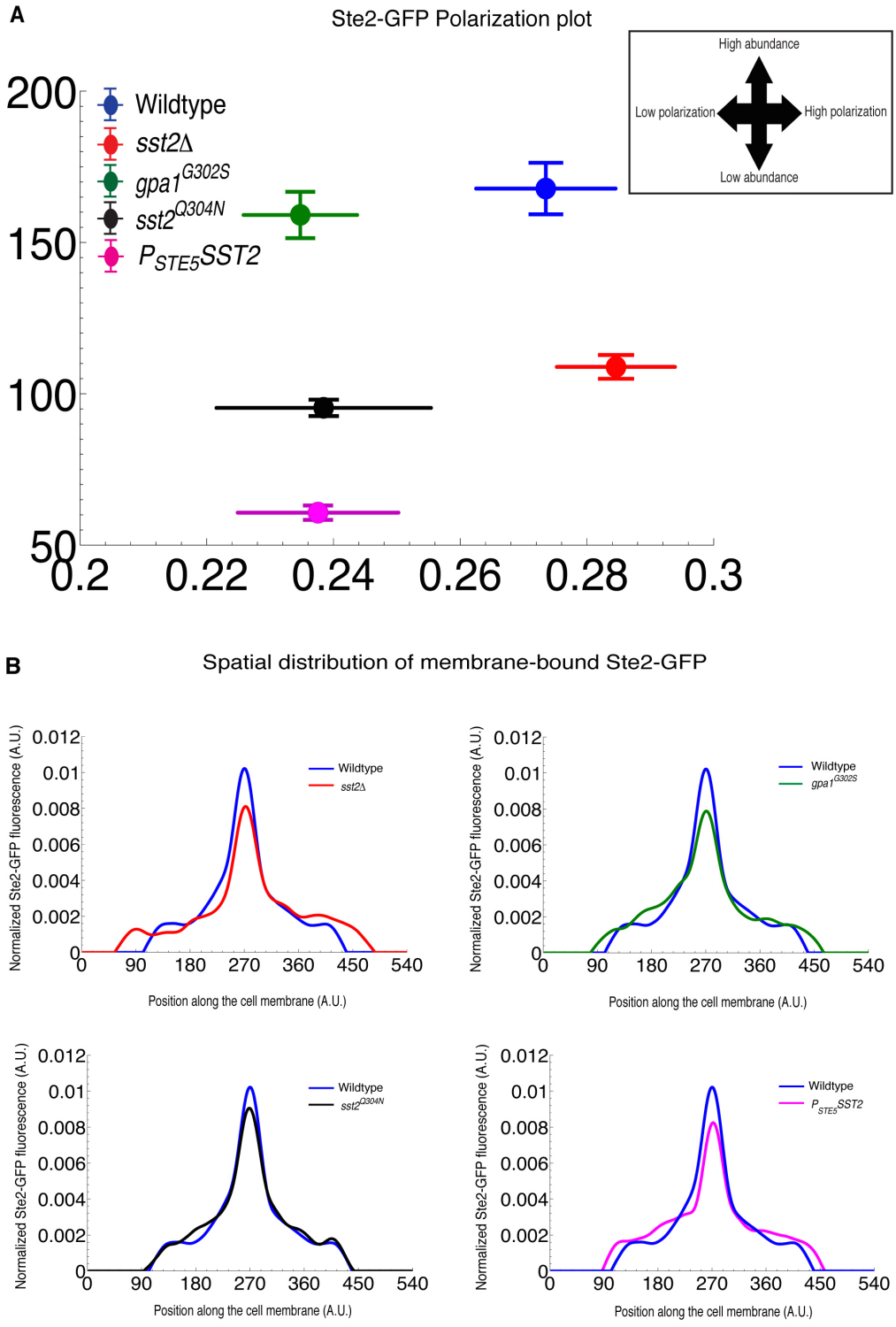

2.3 Discussion

We report here that Sst2 plays a role in the endocytosis and recovery of receptor upon pheromone treatment. In Wildtype cells, we showed that receptor Ste2 undergoes internalization globally and polarizes locally at the growing edge or the shmoo tip later during the pheromone response. We demonstrated that Sst2 is required for Ste2 recovery as cells lacking Sst2 fail to polarize Ste2 at the shmoo tip under high pheromone conditions. Under low pheromone conditions, Ste2 does polarize in *sst2*Δ cells but the amount of a Ste2 on the cell membrane is significantly reduced as compared to the wild type cells. We showed that whole cell Ste2-GFP fluorescence increases in both wild type and *sst2*Δ suggesting that Ste2 is induced in both the cell types but cells lacking Sst2 fail to maintain a stable Ste2 polarization on the cell membrane. The primary function of Sst2 is to act as a GAP for Gα. Here we showed that attenuating the GAP activity of Sst2 by a point mutation (gpa1^{G302S}) enhances Ste2 recovery on the plasma membrane. This suggests that GAP activity does not play a major role in Ste2 recovery except that loss of GAP activity results in elevated levels of Ste2 overall due

---

Figure 2.10: **Sst2 plays a role in Ste2-GFP polarization at the membrane**.
A. A scatter plot showing the affect of Sst2 on Ste2-GFP polarization. Cells were treated with 150 nM pheromone for 3 hours and images were collected at 2min intervals. Ste2-GFP polarization in cells from was measured and the polarization index was plotted against Ste2-GFP on the front half of the cell. Each data point is the mean from last ten time points in the experiment. Error bars denote standard deviation from the mean. Inset shows how different data points in the polarization plot can be compared. B. Spatial distribution of Ste2-GFP in *sst2*Δ, *gpa1*^{G302S}, *sst2*^{Q304N} and P_{STE5}-*SST2* cells compared against Ste2-GFP distribution in wildtype cells by plotting normalized Ste2-GFP fluorescence profile on the membrane against the position on the cell. Each profile is centered at Ste2-GFP peak and the profiles are normalized such that the area under the curve is 1. Ste2-GFP distribution in wildtype cells treated with 150 nM pheromone is shown in blue. Ste2-GFP distribution in *sst2*Δ cells treated with 150 nM pheromone is shown in red. Ste2-GFP distribution in *gpa1*^{G302S} cells treated with 150 nM pheromone is shown in green. Ste2-GFP distribution in *sst2*^{Q304N} cells treated with 150 nM pheromone is shown in black. Ste2-GFP distribution in P_{STE5}-*SST2* cells treated with 150 nM pheromone is shown in magenta.

to hike in induction (more free G$\beta\gamma$). This claim is supported by a higher whole cell Ste2-GFP fluorescence in gpa1^{G302S} cells as compared to the wild type under both low and high pheromone conditions.

Our results demonstrate that Sst2 is required for a stable receptor polarization at the plasma membrane but GAP activity of Sst2 is not required to achieve receptor recovery. This suggests that a novel function for Sst2 in the pheromone dependent endocytosis and recovery of Ste2 exists in the pheromone pathway. In the next chapter we will use mathematical modeling to formulate and test hypotheses to explain our experimental results.

2.4 Methods

2.4.1 Cell growth conditions and strain construction

Standard procedures were followed for yeast media preparation and growth and maintenance of cells. All the strains used in this study were made in BY4741 background. Standard protocols for transformation of yeast and bacteria and manipulation of DNA were used.

Table 2.4 lists the strains used in this chapter. Wildtype BY4741 strain expressing GFP-tagged Ste2 was acquired from the GFP library [41]. The mutant strains *sst2*Δ and *gpa1*^{G302S} were constructed as described previously (Dixit etal, Mol cell (manuscript accepted, awaiting publication) 2014). Ste2-GFP was introduced in these mutant strains by transformation of the linearized pRS-406-STE2-GFP integrating vector as described previously [42]. The mutant strain *sst2*^{Q304N} was constructed as described previously (Dixit etal, Mol cell (manuscript accepted, awaiting publication) 2014). Ste2-GFP was introduced in these mutant strains by transformation of the linearized pRS-406-STE2-GFP integrating vector as described previously [42].

Construction of a strain with constitutively expressed SST2

The *P$_{STE5}$-SST2 STE2-GFP::His3MX6* strain was generated by replacing the portion of the *RIF2-SST2* intergenic region (-1 to -417 from the *SST2* ATG codon) with 815 bp from the *ARX1-STE5* intergenic region (-1 to -815 from the *STE5* ATG codon) in the diploid strain

BYE046. The purpose of the replacement was to detach *SST2* expression from pheromone sensitive gene expression, and *STE5* is suitable replacement as it is constitutively expressed at levels comparable to *SST2* even in the presence of pheromone. A diploid, a cross between the *STE2-GFP::His3MX6* a-type from the GFP collection [41] and BY4742 α-type, was chosen for genetic manipulation because disruptions of *SST2* in haploids selects for suppressor mutations. Using the Delitto Perfetto approach, the *RIF2-SST2* intergenic region was replaced with a P_{SST2}*::CORE-UK* allele in BYE046. pCORE-UK [43] was used for the template in the first round of PCR with the primer pair 1236/1238. The PCR product was then used as template in the second round with primer pair 1237/1239, which extended 60 bp of targeting homologous sequence to each end of the CORE-UK cassette. The amplicon was then transformed into BYE046. Replacement of the *SST2 UAS* region with the CORE-UK cassette was selected for on -Ura medium and confirmed by PCR analysis using genomic DNA as template with primer pairs 1248/881. In the next step, P_{SST2}*::CORE-UK* was replaced with a P_{STE5} fragment containing flanking homology to the intergenic region that was added through successive rounds of PCR. Genomic DNA served as the template for the first round of PCR with primer pair 1242/1244. The PCR product was used as template for a second round of PCR using primer pair 1243/1245. The amplicon, containing 851 bp of sequence from the *STE5* intergenic region, included 61 bp of homology on each end that targeted the fragment to the *SST2* locus. A counter selection with 5 FOA resolved those isolates that either had the cassette replaced or had URA3 activity disrupted through alternative means. Isolates with true replacements of the CORE-UK cassette were confirmed by G418 sensitivity and PCR using genomic DNA as template and primer pair 1248/1147. Sequence fidelity of the P_{STE5}*-SST2* strains were assessed by DNA sequence analysis using the confirmation PCR primers, and a clean isolate was designated BYE047. BYE047 was then sporulated and tetrads dissected. A segregant with appropriate markers, BY4741-161, was preserved and used for microscopy experiments examining the effects of a noninducible *SST2* on STE2 dynamics in response to pheromone. Table 2.5 lists the primers used in the construction of this strain.

Table 2.4:

List of strains used in chapter 2.

Strain	Parent	Description	Source/Reference
Wildtype	BY4741	*MATa STE2-GFP*	GFP library [41]
sst2Δ	BY4741	*MATa STE2-GFP::HIS sst2*Δ*::KanMX4*	This study
gpa1^{G302S}	BY4741	*MATa STE2-GFP::HIS Gpa1G302S::URA3*	This study
sst2^{Q304N}	BY4741	*MATa STE2-GFP::HIS Sst2Q304N*	This study
P_{STE5}-*SST2*	BY4741	*MATa STE-GFP::His3MX6* P_{STE5}-*SST2*	This study

Table 2.5:

List of primers used in chapter 2.

Primer listing	Sequence (5′ 3′)
1236_PSST2CORE_F1	GTACATGATAGATAAATTACCAAGGTCTTT ttcgtacgctgcaggtcgac
1237_PSST2CORE_F2	CAGCGTCTTCCACTTAAGTTAACTCGAAAAGT ACATGATAGATAAATTACC
1238_PSST2CORE_R1	TTCATGCAACGTCCTATTTTTATCCACCATCC GCGCGTTGGCCGATTCAT
1239_PSST2CORE_R2	CGGCGTTCTGCTGAAATTTTTGGAAGATAATTC ATGCAACGTCCTATTTT
1242_PSTE5SST2_F1	GTACATGATAGATAAATTACCAAGGTCTTTAGCT CATCTCATCTCTTCTGCTG
1243_PSTE5SST2_F2	CCAGCGTCTTCCACTTAAGTTAACTCGAAAAGT ACATGATAGATAAATTACC
1244_PSTE5SST2_R1	CATGCAACGTCCTATTTTTATCCACCATTTAAAA GTTGTTTCCGCTGTATCC
1245_PSTE5SST2_R2	CCATTCGGCGTTCTGCTGAAATTTTTGGAAGATA ATTCATGCAACGTCCTATTTTTATCC

2.4.2 Live-cell imaging and microfluidics

Ste2 endocytosis was measured by monitoring the fluorescence of GFP tagged Ste2 on the cell membrane, following pheromone stimulation. Overnight starter cultures were diluted twice. The second dilution is made in 5 milliliter of synthetic complete medium with dextrose (SCD) and the cells were grown in an incubator shaker at 30°C till the OD_{600} reached approximately 0.2. The live-cell imaging experiment was carried out in a microfluidic device described previously [14]. Cells were loaded into the cell trap through the cell port c (Figure A.1 A). The microfluidic device is mounted on an Olympus microscope with Yokogawa Spinning Disk and EMCCD Camera for live cell imaging. Stage positions to be mon-

itored during the time course were set using an ASI PZ-2000 XYZ Series Automated stage with Piezo Z-axis top plate (http://asiimaging.com/products/stages/inverted-stages/pz-2000-xyz-automated-stage-with-piezo-z-axis-top-plate/). Pheromone was introduced into chamber by raising the ports containing pheromone (P1, P2) and lowering the ports containing plain media (M1, M2) (Figure A.1 B). Differential Inference Contrast (DIC) and fluorescence images were acquired at 2min intervals at 100X magnification using MetaMorph software (http://www.moleculardevices.com/). Image processing was done in ImageJ (http://rsbweb.nih.gov/ij/) and the quantification of Ste2 was performed in MATLAB (http://www.mathworks.com).

2.4.3 Quantification of membrane bound Ste2 from fluorescence microscopy images

Raw DIC images from microscopy experiments were loaded into ImageJ. Cell boundaries were identified manually and saved in ImageJ ROI Manager (Figure A.2 A). Raw fluorescence images from the same experiment were then loaded into ImageJ. The background fluorescence was subtracted using a standard background subtraction algorithm in ImageJ with a rolling ball radius of 150 pixels. The cell boundaries identified using DIC images were used to calculate Ste2 membrane intensity from fluorescence images. For each cell, an annular ring encompassing the cell membrane was created by shrinking the cell boundary (red circle) by 3 pixels (cyan circle) (Figure A.2 B). The intensity of Ste2 on the cell membrane was calculated as the difference between intensities inside red and cyan circles (Figure A.2 C). The time-series of fluorescence intensities of membrane bound Ste2 in each cell is plotted. Mean and standard deviations of all the single cell time-series were calculated to generate a mean fluorescence intensity profile of membrane bound Ste2.

2.4.4 Comparision of Ste2-GFP in different strains at steady state

Measured Ste2-GFP fluorescence varies with fluctuations in the laser intensity between each experiment day. In order to compare Ste2-GFP fluorescence across different strains, we sought to normalize the fluctuations in laser intensity between experiments done on different

days by measuring steady state Ste2-GFP fluorescence in cells simultaneously. Overnight starter cultures of all the strains used in the study were diluted twice. The second dilution was made in 5ml of synthetic complete medium with dextrose (SCD) lacking appropriate amino acids. The cells were grown in an incubator shaker at 30°C till the OD_{600} reached 0.2. 10μl of cells were plated on 2% agarose pads and covered with a cover glass (Cornig Microscope Cover Glass). The agar pads were mounted on an Olympus microscope described in the live-cell imaging section above and fluorescence images were acquired at 100X magnification using MetaMorph software. Background subtraction and cell boundary identification was done in ImageJ ((http://rsbweb.nih.gov/ij/) and annular rings of 3 pixel width were created. Ste2-GFP amount on the membrane was measured as the fluorescence intensity in the annular rings. A box plot was created for membrane bound Ste2-GFP levels measured for each strain. Since the cells were not treated with pheromone, the box plot thus created is a measure of the steady state Ste2-GFP in the strains. Student t-test was conducted to confirm if the steady state receptor levels in different strains are significantly different from the wildtype strain.

2.4.5 Peak width of membrane bound Ste2

The length of the Ste2 polar cap was quantified as the full width at half maximum (FWHM) of Ste2-GFP peak on the membrane. Membrane masks were created in MATLAB for each cell and Ste2-GFP pixel values in the membrane region were measured and a profile of Ste2-GFP along the membrane was created. Ste2-GFP profile along the membrane for each cell at every time point was aligned to the center of the respective Ste2-GFP peak. The profiles were normalized such that the area under each profile is 1. A threshold was applied to the average of normalized Ste2-GFP profiles to find the average Ste2-profile 20% above the background. The thresholded Ste2-GFP profile was normalized again such the area under the profile is 1 and then fit to a Gaussian to find the FWHM.

2.4.6 Mathematical Modeling

We modeled the role of Sst2 in the internalization of membrane bound Ste2 in yeast cells upon pheromone treatment. We developed an ODE-based mathematical model, which takes pheromone stimulus as the input and computes the time course of Ste2 abundance. The canonical model consists of a system of 8 coupled ODEs and 34 parameters. The differential endocytosis model consists of a system of ten coupled ODEs and 36 parameters, which were solved using the ode15s solver in MATLAB. A stiff solver (ode15s) is used in solving this system of ODEs as there are events occurring at multiple time scales. See Appendix B for the detailed set of equations and the list of parameters in the model. Initial estimates for the parameters were either chosen from literature or were assigned by us to match the experimental steady state levels of proteins in wild type cells. Parameter estimation was performed to find the parameters that best fit experimental data.

2.4.7 Parameter Estimation

Parameter estimation was performed using a modified evolutionary algorithm as described previously in [44]. The model was trained with Ste2-GFP time course data of wildtype and sst2Δ cells treated with 150nM pheromone. For training the model, 12 instances of the algorithm was run in parallel, each starting with 6 different sets of parent parameter values. Half of the initial parent parameter sets are the best guess parameters from literature and steady state protein levels and the remaining half were sets of randomly chosen values. In the algorithm, p was set to 6, C=6, μ=30%, λ=10% and β=0.75. The algorithm was run for 2000 generations, which resulted in 0.86 million trials in the parameter search. Top 50 scored parameter sets were used to validate remaining data sets and make testable predictions. See Appendix B for the parameter estimation results.

2.4.8 Model Robustness

The quality of a mathematical model and the reliability of its predictions depend on model robustness. Since the behavior of a model is highly dependent on the choice of parameter values, one should be aware if the predictions made are valid over a wide range of parameter values or the predictions are highly sensitive to perturbations in the concerned parameters. One way to test the robustness of a model is to identify the parameter sets that best fit the data and calculate the variance in the distribution of each parameter. Top 50 parameter sets from the evolutionary algorithm run (described above) were collected and histograms of each parameter was generated. Coefficient of variation of each parameter was reported in increasing order (Most sensitive or highly constrained parameters to least sensitive or robust parameters).

CHAPTER 3

CONCLUSIONS AND FUTURE DIRECTIONS

Previous studies have established Sst2 as an important negative regulator in the pheromone response pathway [11]. Sst2 belongs to the family of Regulator of G-protein Signaling (RGS) proteins that negatively regulate G-proteins by the GTPase activating protein (GAP) activity of their RGS domain [20]. In the present work, we have demonstrated a novel positive role for Sst2 in the mating response. We have presented data demonstrating that Ste2 polarization is absent in $sst2\Delta$ cells treated with saturating concentration of pheromone. Based on a previous observation that Sst2 interacts with Ste2 and that the site of Sst2 localization on the cell membrane precludes phosphorylation of Ste2 by kinases Yck1/2 [21], we formulated a hypothesis that Sst2 binds Ste2, inhibits its endocytosis and stabilizes Ste2 at the plasma membrane to form of a stable polarized Ste2 distribution. We developed a mathematical model to test our differential endocytosis model. Even though the canonical model for Ste2 internalization captures the recovery of Ste2 at the plasma membrane in wildtype cells, it fails to capture the loss of Ste2 recovery in $sst2\Delta$ cells at high pheromone concentration. Whereas, our differential endocytosis model was able to reproduce the time course data of Ste2 profiles in wildtype and $sst2\Delta$ cells at both saturating and low levels of pheromone. The model was validated by disrupting the binding interaction between Sst2 and Ste2 through a point mutation in $sst2^{Q304N}$. As expected from our model, Ste2 did not form a stable polarized distribution in $sst2^{Q304N}$ cells when treated with saturating concentrations of pheromone. An important prediction of our model was that the induction of Sst2 is required for the polarized recovery of Ste2 on the

plasma membrane following exposure to pheromone. We tested the prediction by replacing the endogenous SST2 promoter with a STE5 promoter, which doesnt undergo pheromone-induced transcription. The promoter replacement was chosen so as to maintain the same level of basal expression of Sst2. Cells expressing Sst2 at basal level constitutively showed less recovery of Ste2 at the plasma membrane compared to wildtype cells, supporting our model prediction that Sst2 induction is an important factor in establishing a stable polarized Ste2 distribution. We have also shown that in addition to the amount of Ste2, the extent of polarization (measured as the polarization index) is different in the strains used in the study. We believe that Sst2 reduces the extent of Ste2 phosphorylation by casein kinases Yck1/2 by competing for binding to Ste2. Contrary to the speculation that Sst2 binds unphosphorylated receptor [21] we believe Yck1/2 phosphorylate only those receptors not bound to Sst2. Polarized active $G\alpha$ [23] leads to the polarization of Sst2 at the presumptive shmoo site. Pheromone induced directed transport of Ste2 occurs at the site of $G\beta\gamma$ polarization, i.e., shmoo site. Sst2 binds Ste2 at the shmoo site and blocks its phosphorylation and hence its internalization, thereby stabilizing Ste2 at the shmoo site. In the context of gradient sensing, absence of a stable polarization of Ste2 at the front end of cells lacking Sst2 may lead to an unstable polarization of $G\beta\gamma$, if any. This transient polarization of $G\beta\gamma$ could play a role in the turning of $sst2\Delta$ cells in a gradient [25], decreasing the efficiency of gradient sensing. Thus the novel role of Sst2 in blocking Ste2 endocytosis as demonstrated here could play a positive role in gradient sensing. Since GPCR signaling pathways are conserved between yeast and mammalian systems, the role of RGS proteins in regulating GPCR trafficking by inhibition of receptor internalization could be a general occurrence in GPCR signaling.

Appendix A

SUPPLEMENTARY MATERIAL FOR CHAPTER 2

A.1 Microfluidics for live-cell imaging

Figure A1 describes the schematic of the microfluidics device used in the study, along with the steps involved in using the device for live cell imaging.

A.2 Image analysis procedure to calculate membrane bound Ste2-GFP

Figure A2 describes the image analysis scheme employed for the quantification of live cell microscopy data. All the steps described here were performed in ImageJ.

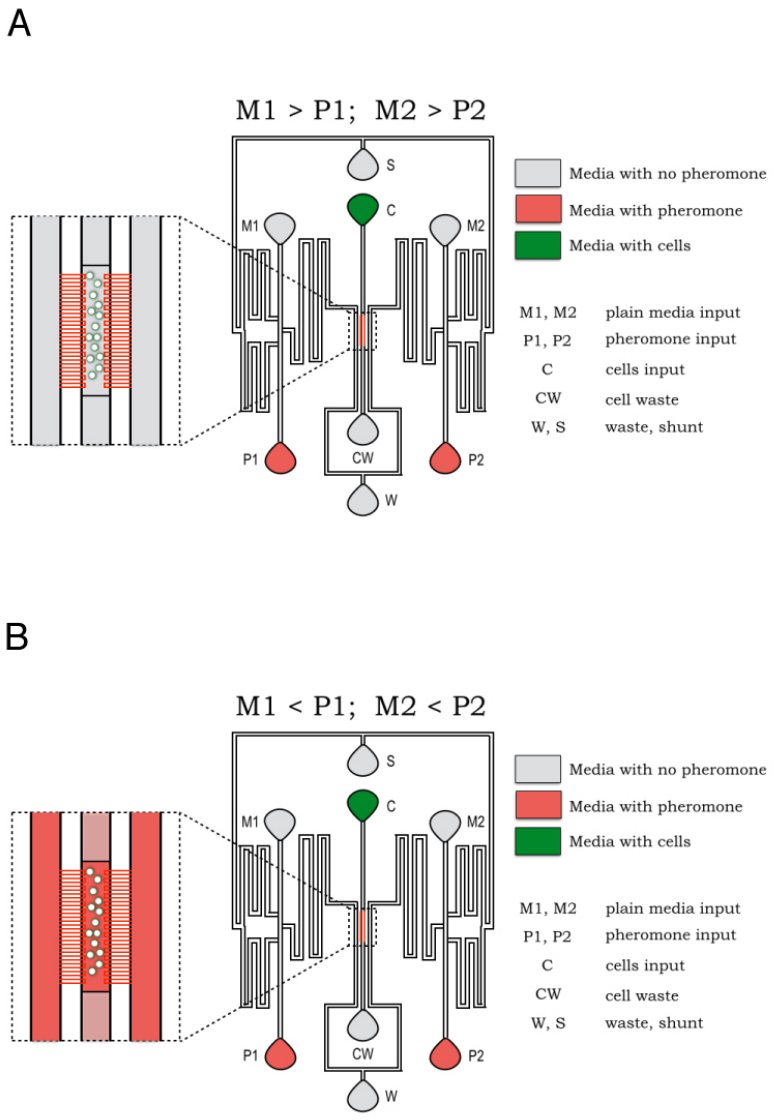

Figure A.1: A. Yeast cells for live-cell imaging loaded in to the cell chamber using the cell loading port 'c'. Cells are not exposed to pheromone at this stage as the ports containing media (M1, M2) are kept higher than ports containing media + pheromone (P1,P2). B. Pheromone is introduced into the cell chamber by raising ports P1 and P2 and lowering ports M1 and M2. Pheromone enters the cell chamber and distributes uniformly by diffusion.

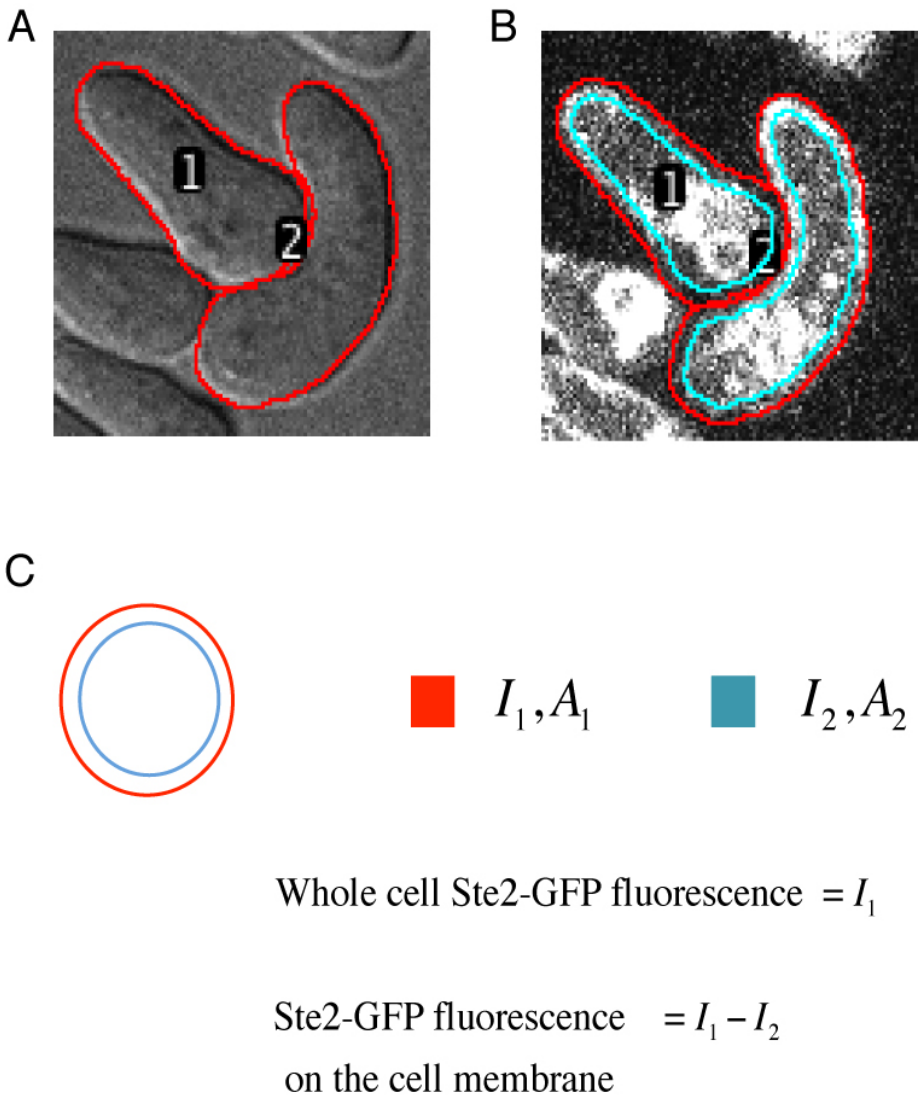

Figure A.2: A. Cell boundaries (red circles) identified manually and saved in ImageJ ROI Manager. B. The cell boundary (red circle) was shrinked by 3pixels (cyan circle) to create an annular ring around the cell membrane. C. Measurement of Ste2-GFP on the cell membrane : Fluorescence intensity in the annular ring is a measure of Ste2-GFP on the cell membrane. Whole cell Ste2-GFP : Fluorescence intensity inside the red circle is a measure of Ste2-GFP in the cell as a whole.

BIBLIOGRAPHY

[1] M. J. Marinissen and J. Gutkind, "G-protein-coupled receptors and signaling networks: emerging paradigms," *Trends in Pharmacological Sciences*, vol. 22, no. 7, pp. 368 – 376, 2001. 1

[2] H. A. Rockman, W. J. Koch, and R. J. Lefkowitz, "Seven-transmembrane-spanning receptors and heart function," *Nature*, vol. 415, pp. 206–212, 01 2002. 1

[3] J. P. Overington, B. Al-Lazikani, and A. L. Hopkins, "How many drug targets are there?," *Nat Rev Drug Discov*, vol. 5, pp. 993–996, 12 2006. 1

[4] E. M. Ross and T. M. Wilkie, "Gtpase-activating proteins for heterotrimeric g proteins: Regulators of g protein signaling (rgs) and rgs-like proteins," *Annual Review of Biochemistry*, vol. 69, no. 1, pp. 795–827, 2000. PMID: 10966476. 1

[5] B. Sjögren, L. L. Blazer, and R. R. Neubig, "Regulators of g protein signaling proteins as targets for drug discovery," in *Membrane Proteins as Drug Targets* (C. A. Lunn, ed.), vol. 91 of *Progress in Molecular Biology and Translational Science*, ch. 4, pp. 81 – 119, Academic Press, 2010. 1

[6] T. Wieland, S. Lutz, and P. Chidiac, "Regulators of g protein signalling: a spotlight on emerging functions in the cardiovascular system," *Current Opinion in Pharmacology*, vol. 7, no. 2, pp. 201 – 207, 2007. Cardiovascular and renal. 1

[7] P. Zhang and U. Mende, "Regulators of g-protein signaling in the heart and their potential as therapeutic targets," *Circulation Research*, vol. 109, no. 3, pp. 320–333, 2011. 1

[8] S. Tsang, A. Woo, W. Zhu, and R. Xiao, "Deregulation of rgs2 in cardiovascular diseases.," *Frontiers in bioscience (Scholar edition)*, vol. 2, pp. 547–557, 2010. 1

[9] C. Nunn, M.-X. Zou, A. J. Sobiesiak, A. A. Roy, L. A. Kirshenbaum, and P. Chidiac, "Rgs2 inhibits βadrenergic receptor-induced cardiomyocyte hypertrophy," *Cellular Signalling*, vol. 22, no. 8, pp. 1231 – 1239, 2010. 1

[10] K. Chakir, W. Zhu, S. Tsang, A. Y.-H. Woo, D. Yang, X. Wang, X. Zeng, M.-H. Rhee, U. Mende, N. Koitabashi, E. Takimoto, K. J. Blumer, E. G. Lakatta, D. A. Kass, and R.-P. Xiao, "Rgs2 inhibits βadrenergic receptor-induced cardiomyocyte hypertrophy is a primary terminator of β2adrenergic receptor-mediated gi signaling," *Journal of Molecular and Cellular Cardiology*, vol. 50, no. 6, pp. 1000 – 1007, 2011. 1

[11] H. G. Dohlman, J. Song, D. Ma, W. E. Courchesne, and J. Thorner, "Sst2, a negative regulator of pheromone signaling in the yeast saccharomyces cerevisiae: expression, localization, and genetic interaction and physical association with gpa1 (the g-protein alpha subunit).," *Molecular and Cellular Biology*, vol. 16, no. 9, pp. 5194–209, 1996. 1, 3, 41

[12] F. Cross, L. H. Hartwell, C. Jackson, and J. B. Konopka, "Conjugation in saccharomyces cerevisiae," *Annual Review of Cell Biology*, vol. 4, no. 1, pp. 429–455, 1988. PMID: 2848554. 2

[13] J. E. Segall, "Polarization of yeast cells in spatial gradients of alpha mating factor," *Proceedings of the National Academy of Sciences*, vol. 90, no. 18, pp. 8332–8336, 1993. 2, 4

[14] N. Hao, S. Nayak, M. Behar, R. H. Shanks, M. J. Nagiec, B. Errede, J. Hasty, T. C. Elston, and H. G. Dohlman, "Regulation of cell signaling dynamics by the protein kinase-scaffold ste5," *Molecular Cell*, vol. 30, no. 5, pp. 649 – 656, 2008. 2, 36

[15] K. Schrick, B. Garvik, and L. H. Hartwell, "Mating in saccharomyces cerevisiae: The role of the pheromone signal transduction pathway in the chemotropic response to pheromone," *Genetics*, vol. 147, no. 1, pp. 19–32, 1997. 2

[16] E. A. Elion, "Pheromone response, mating and cell biology," *Current Opinion in Microbiology*, vol. 3, no. 6, pp. 573 – 581, 2000. 2

[17] Y. Wang and H. G. Dohlman, "Pheromone signaling mechanisms in yeast: A prototypical sex machine," *Science*, vol. 306, no. 5701, pp. 1508–1509, 2004. 2

[18] L. Bardwell, "A walk-through of the yeast mating pheromone response pathway," *Peptides*, vol. 25, no. 9, pp. 1465 – 1476, 2004. M. Altstein. 2

[19] R. A. Arkowitz, "Chemical gradients and chemotropism in yeast," *Cold Spring Harbor Perspectives in Biology*, vol. 1, no. 2, 2009. 3

[20] D. M. Apanovitch, K. C. Slep, P. B. Sigler, and H. G. Dohlman, "Sst2 is a gtpase-activating protein for gpa1: Purification and characterization of a cognate rgsgα protein pair in yeast," *Biochemistry*, vol. 37, no. 14, pp. 4815–4822, 1998. 3, 41

[21] D. R. Ballon, P. L. Flanary, D. P. Gladue, J. B. Konopka, H. G. Dohlman, and J. Thorner, "Dep-domain-mediated regulation of {GPCR} signaling responses," *Cell*, vol. 126, no. 6, pp. 1079 – 1093, 2006. 3, 4, 9, 13, 20, 27, 41, 42

[22] D. D. Jenness, A. C. Burkholder, and L. H. Hartwell, "Binding of -factor pheromone to yeast a cells: Chemical and genetic evidence for an -factor receptor," *Cell*, vol. 35, no. 2, Part 1, pp. 521 – 529, 1983. 4

[23] D. V. Suchkov, R. DeFlorio, E. Draper, A. Ismael, M. Sukumar, R. Arkowitz, and D. E. Stone, "Polarization of the yeast pheromone receptor requires its internalization but not actin-dependent secretion," *Molecular Biology of the Cell*, vol. 21, no. 10, pp. 1737–1752, 2010. 4, 8, 30, 42

[24] C. J. Stefan and K. J. Blumer, "A syntaxin homolog encoded by vam3 mediates down-regulation of a yeast g protein-coupled receptor," *Journal of Biological Chemistry*, vol. 274, no. 3, pp. 1835–1841, 1999. 4, 9

[25] T. I. Moore, C.-S. Chou, Q. Nie, N. L. Jeon, and T.-M. Yi, "Robust spatial sensing of mating pheromone gradients by yeast cells," *PLoS ONE*, vol. 3, p. e3865, 12 2008. 4, 42

[26] E. Marco, R. Wedlich-Soldner, R. Li, S. J. Altschuler, and L. F. Wu, "Endocytosis optimizes the dynamic localization of membrane proteins that regulate cortical polarity," *Cell*, vol. 129, pp. 411–422, 2014/05/17 2007. 4

[27] S. J. Altschuler, S. B. Angenent, Y. Wang, and L. F. Wu, "On the spontaneous emergence of cell polarity," *Nature*, vol. 454, pp. 886–889, 08 2008. 4

[28] J. Valdez-Taubas and H. R. B. Pelham, "Slow diffusion of proteins in the yeast plasma membrane allows polarity to be maintained by endocytic cycling," *Current Biology*, vol. 13, pp. 1636–1640, 2014/05/17 2003. 4

[29] L. Vallier, J. Segall, and M. Snyder, "The alpha-factor receptor C-terminus is important for mating projection formation and orientation in Saccharomyces cerevisiae," *CELL MOTILITY AND THE CYTOSKELETON*, vol. 53, pp. 251–266, DEC 2002. 4, 8

[30] L. Hicke, B. Zanolari, and H. Riezman, "Cytoplasmic tail phosphorylation of the -factor receptor is required for its ubiquitination and internalization," *The Journal of Cell Biology*, vol. 141, no. 2, pp. 349–358, 1998. 4

[31] K. A. Schandel and D. D. Jenness, "Direct evidence for ligand-induced internalization of the yeast alpha-factor pheromone receptor.," *Molecular and Cellular Biology*, vol. 14, no. 11, pp. 7245–7255, 1994. 4

[32] D. D. Jenness and P. Spatrick, "Down regulation of the -factor pheromone receptor in s. cerevisiae," *Cell*, vol. 46, no. 3, pp. 345 – 353, 1986. 4, 10

[33] M. Rodríguez-Muñoz, E. de la Torre-Madrid, G. Gaitán, P. Sánchez-Blázquez, and J. Garzón, "Rgs14 prevents morphine from internalizing mu-opioid receptors in periaqueductal gray neurons," *Cellular Signalling*, vol. 19, no. 12, pp. 2558 – 2571, 2007. 4

[34] J. Celver, M. Sharma, and A. Kovoor, "Rgs9-2 mediates specific inhibition of agonist-induced internalization of d2-dopamine receptors," *Journal of Neurochemistry*, vol. 114, no. 3, pp. 739–749, 2010. 4

[35] J. B. Konopka, D. D. Jenness, and L. H. Hartwell, "The c-terminus of the s. cerevisiae ?-pheromone receptor mediates an adaptive response to pheromone," *Cell*, vol. 54, pp. 609–620, 2014/06/04 1988. 8

[36] D. Pruyne, A. Legesse-Miller, L. Gao, Y. Dong, and A. Bretscher, "Mechanisms of polarized growth and organelle segregation in yeast," *Annual Review of Cell and Developmental Biology*, vol. 20, no. 1, pp. 559–591, 2004. PMID: 15473852. 8

[37] A. Kovoor, P. Seyffarth, J. Ebert, S. Barghshoon, C.-K. Chen, S. Schwarz, J. D. Axelrod, B. N. R. Cheyette, M. I. Simon, H. A. Lester, and J. Schwarz, "D2 dopamine receptors colocalize regulator of g-protein signaling 9-2 (rgs9-2) via the rgs9 dep domain, and rgs9

knock-out mice develop dyskinesias associated with dopamine pathways," *The Journal of Neuroscience*, vol. 25, no. 8, pp. 2157–2165, 2005. 9

[38] J. Celver, M. Sharma, and A. Kovoor, "Rgs9-2 mediates specific inhibition of agonist-induced internalization of d2-dopamine receptors," *Journal of Neurochemistry*, vol. 114, no. 3, pp. 739–749, 2010. 10, 13

[39] N. Yildirim, N. Hao, H. G. Dohlman, and T. C. Elston, "Mathematical modeling of $\{$RGS$\}$ and g-protein regulation in yeast," in *Regulators of G-Protein Signaling, Part A* (D. P. Siderovski, ed.), vol. 389 of *Methods in Enzymology*, pp. 383 – 398, Academic Press, 2004. 12, 19

[40] T.-M. Yi, H. Kitano, and M. I. Simon, "A quantitative characterization of the yeast heterotrimeric g protein cycle," *Proceedings of the National Academy of Sciences*, vol. 100, no. 19, pp. 10764–10769, 2003. 19

[41] W.-K. Huh, J. V. Falvo, L. C. Gerke, A. S. Carroll, R. W. Howson, J. S. Weissman, and E. K. O'Shea, "Global analysis of protein localization in budding yeast," *Nature*, vol. 425, pp. 686–691, 10 2003. 34, 35, 36

[42] G. Dixit, R. Baker, C. M. Sacks, M. P. Torres, and H. G. Dohlman, "Guanine nucleotide-binding protein (gα) endocytosis by a cascade of ubiquitin binding domain proteins is required for sustained morphogenesis and proper mating in yeast," *Journal of Biological Chemistry*, vol. 289, no. 21, pp. 15052–15063, 2014. 34

[43] F. Storici and M. A. Resnick, "The delitto perfetto approach to in vivo sitedirected mutagenesis and chromosome rearrangements with synthetic oligonucleotides in yeast," in *DNA Repair, Part B* (J. L. Campbell and P. Modrich, eds.), vol. 409 of *Methods in Enzymology*, pp. 329 – 345, Academic Press, 2006. 35

[44] Y. Fu, S. Lim, D. Urano, M. Tunc-Ozdemir, N. G. Phan, T. C. Elston, and A. M. Jones, "Reciprocal encoding of signal intensity and duration in a glucose-sensing circuit," *Cell*, vol. 156, no. 5, pp. 1084 – 1095, 2014. 39